AAPS PharmSciTech (2026) 27:269
https://doi.org/10.1208/s12249-026-03512-5

RESEARCH ARTICLE

Syringic Acid–Loaded Emulsomes as a Neuroprotective Delivery System: Formulation Optimization and *In-Vivo* Pharmacokinetic Evaluation

Nabila M. Sweed[1] · **Mahitab H. Elbishbishy**[2] · **Sara S. Saleh**[3] · **Marwa H. S. Dawoud**[1]

Received: 12 March 2026 / Accepted: 30 June 2026

Abstract

Syringic acid (SA) demonstrates significant anti-inflammatory, antioxidant, and neuroprotective properties. Unfortunately, its clinical applicability is limited by low solubility and low bioavailability. SA-loaded emulsomes were developed to overcome these limitations. The emulsomes were prepared using thin-film hydration method and optimized by a Central Composite Design. Three independent variables were studied: the solid lipid-to-phosphatidylcholine ratio, drug amount, and solid lipid type (trilaurin or tripalmitin). The measured responses were entrapment efficiency (EE%), particle size (PS), and zeta potential (ZP). The optimized formula exhibited an EE% of 61.92 ± 0.09%, a PS of 190.02 ± 0.13 nm, a PDI of 0.21 ± 0.07 and a ZP of –36.3 ± 0.98 mV. *In-vitro* release studies demonstrated a sustained release profile, with 92% of SA released over 24 h. The relative bioavailability of SA from the optimized formula was 219% compared to the unformulated drug. A physiologically based pharmacokinetic (PBPK) model was developed to predict plasma and tissue distribution. The model predicted a twofold increase in brain bioavailability, suggesting the potential for improved brain penetration and retention. These findings establish emulsomes as a promising nanoplatform for overcoming syringic acid's biopharmaceutical barriers and advancing its clinical potential.

Keywords central composite design · emulsomes · syringic acid · trilaurin · tripalmitin

Introduction

Oxidative stress, resulting from an imbalance between the cellular antioxidant defence system and the excessive production of reactive oxygen species (ROS) such as superoxide (O_2^-), hydroxyl radicals (•OH), and hydrogen peroxide (H_2O_2), plays a critical role in the pathogenesis of neurodegenerative disorders including Parkinson's, Alzheimer's, and Huntington's diseases. These ROS induce DNA damage, neuronal loss, and inflammatory responses, thereby accelerating neurodegeneration [1–3].

Plant-derived polyphenols have gained considerable attention for their neuroprotective potential due to their antioxidant, anti-inflammatory, and anti-apoptotic activities, primarily through scavenging ROS generated during oxidative stress [4, 5].

Among them, syringic acid (SA; 4-hydroxy-3,5-dimethoxybenzoic acid) is a naturally occurring polyphenol with demonstrated antioxidant and neuroprotective effects. Its activity is attributed to its chemical structure, particularly the presence of methoxy groups that enhance free radical

The manuscript has not been published and is not under consideration for publication elsewhere.

✉ Nabila M. Sweed
nabila.msweed@gmail.com; nsueed@msa.edu.eg

[1] Department of Pharmaceutics, Faculty of Pharmacy, October University for Modern Sciences and Arts, 26 July Mehwar Road Intersection With Wahat Road, 6th of October, Giza, Egypt

[2] Department of Pharmacognosy, Faculty of Pharmacy, October University for Modern Sciences and Arts, 26 July Mehwar Road Intersection With Wahat Road, 6th of October, Giza, Egypt

[3] Department of Analytical Chemistry, Faculty of Pharmacy, October University for Modern Sciences and Arts, 26 July Mehwar Road Intersection With Wahat Road, 6th of October, Giza, Egypt

Published online: 08 September 2026

scavenging capacity. SA has been shown to reduce oxidative stress, inhibit inflammatory cytokines, and protect against neuronal damage in various models [6–10].

Despite these promising properties, the clinical application of SA is strictly limited by its poor aqueous solubility, rapid *in-vivo* metabolism, and low systemic bioavailability, necessitating the development of advanced delivery systems to improve its pharmacokinetic profile [11, 12].

While polymeric nanoparticles have been explored for brain delivery due to their nanoscale size, they frequently generate acidic or toxic degradation by-products, rendering them unsuitable for long-term neurological therapies [13–16]. Consequently, biocompatible lipid-based nanoparticles (LNPs) have emerged as safer alternatives [17–19]. Previous attempts to optimize SA delivery using nano formulations such as conventional liposomes and self-microemulsifying drug delivery systems (SMEDDS) have been reported, yet they offer limited success due to structural and stability-related drawbacks. SMEDDS may undergo premature drug precipitation upon dilution in the gastrointestinal (GI) tract, while conventional liposomes suffer from rapid drug leakage and high instability in gastric fluid due to their fluid bilayer membranes. These limitations result in a short circulation half-life time and insufficient pharmacokinetic exposure at the target brain tissue [13, 20, 21]. To address these challenges, the present study utilizes emulsomes (cholesterol-stabilized, hybrid lipid nanocarriers) that integrate the structural advantages of liposomes and emulsions within a unique core–shell architecture. Unlike previous fluid-core or micellar formulations, emulsomes possess a solid triglyceride core enveloped by a phospholipid bilayer. This solid core physically immobilizes lipophilic molecules, effectively preventing the rapid drug leakage and burst release characteristic of liposomes. Furthermore, emulsomes offer clear superiority in manufacturing, scalability, and brain pharmacokinetic exposure. For oral administration, the solid lipid core acts as a shield, resisting gastric enzymatic degradation and protecting the encapsulated SA through the GI tract [22–26].

Crucially, the structural similarity of emulsomes to endogenous chylomicrons promotes intestinal lymphatic uptake. This bypasses hepatic first-pass metabolism, thereby increasing systemic maximum concentration in plasma (C_{max}) and bioavailability compared to free SA or conventional SMEDDS. Once in circulation, their nanoscale size and lipidic composition facilitate interaction with the blood–brain barrier (BBB) via passive diffusion and receptor-mediated transcytosis, achieving effective neuroprotective delivery via a non-invasive route suited for chronic therapy [27–29].

Accordingly, this study aims to develop and optimize syringic acid-loaded emulsomes using a Central Composite Design. By establishing a direct structural advantage over previously reported nano formulations, this work seeks to enhance SA solubility, gastric stability, and systemic bioavailability, ultimately providing an efficient oral nanoplatform for the management of neurodegenerative diseases.

Materials and Methods

Plant Material

5.4 kg of the fresh fruits of *Vitis vinifera L.* cv. Flame Seedless family Vitaceae (Red grapes) were purchased from the farms of Faculty of Agriculture, Cairo University, Giza, Egypt, where; the authentication and taxonomical identity were kindly checked and verified by the vegetables and fruits department at the faculty. The fruits were isolated, homogenized, then, freeze-dried under vacuum using a lyophilizer (Freeze Dryer-CHRIST-ALPHA 2–4 LD PLUS).

Chemicals

90% Soybean lecithin was purchased from Alfa Aesar (Germany). Cholesterol, tripalmitin, trilaurin, and vanillic acid (used as an internal standard) were procured from Sigma-Aldrich Chemical Co. (St. Louis, IL, USA). Sigma-Aldrich (USA) also supplied the solvents: HPLC-grade methanol, and analytical-grade acetic acid and formic acid. All remaining chemicals were of analytical grade and used without further purification.

Animals

The current study included male Wistar albino rats, each weighing 200 g. Rats were kept in plastic cages at October University for Modern Science and Arts' animal house under continuous conditions of 25 ± 3 ◦C and 50% humidity after being obtained from Teodor Bilharis Institute in Cairo, Egypt. Water and a standard pellet diet were freely available for the duration of the study.

Methods

Extraction and Isolation of Syringic Acid

The dried fruits (982 g) were macerated at room temperature in 60% ethanol till exhaustion. The hydro-ethanolic extracts were pooled and concentrated in a rotatory evaporator (Heidolph, Germany) under reduced pressure at a temperature not exceeding 60 °C to yield a dark reddish-brown extract weighing (113 g). The dried extract was defatted using hexane (10×50 mL), the defatted extract (89 g) was then extracted with 2M sodium hydroxide and left at room temperature with frequent agitation

for 8 h. The extract was further acidified with 6 M HCl to reach the pH of 2.2. After acidification, the extract was suspended in distilled water (500 mL) and partitioned successively between water dichloromethane (10×50mL), ethyl acetate (10×50mL), and saturated n-butanol (10×50mL). The solvents were distilled-off under reduced pressure to yield 12.8 g, 23.3 g and 14.7 g of the dichloromethane, ethyl acetate, and n-butanol extracts, respectively.

The ethyl acetate fraction (23.3 g) was further fractionated on a polyamide (E-Merck) (100 g, 100×5 cm) column, eluted with 0% up to 100% methanol in distilled water in a 25% gradient elution manner. Fractions were collected each 20 mL and monitored by TLC on silica gel 60 F 254 (E-Merck) precoated plates. Similar fractions were pooled and separately concentrated under reduced pressure at a temperature not exceeding 60 °C, to yield three sub-fractions (I-III), fraction I, eluted with 100% distilled water (1.7 g), fraction II eluted with 50% methanol (6.3 g) and fraction III, eluted with 75% methanol (4.8 g). Fraction III was further fractionated over a column chromatography (50 cm×3.5 cm) packed with Sephadex LH-20 (E-Merck) as a stationary phase. The column was eluted with 0% up to 100% methanol in distilled water in a 10% gradient elution manner. Fractions were collected each 5 mL and monitored by paper chromatography and n-butanol – acetic acid – water (4:1:5) (upper phase) as a solvent system. The column yielded 4 major subfractions of which fraction III-c was obtained as an off-white amorphous powder.

Experimental Design

A Central Composite Design was used to monitor the effects of the various independent variables on the prepared emulsomal characteristics, using Design Expert® software (Version 10, Stat-Ease Inc., Minneapolis, MN). The independent variables were X_1: solid lipid to phosphatidyl choline ratio (SL:PC) (X_2): drug amount (mg), and (X_3): type of solid lipid, whereas the dependant variables were the entrapment efficiency percentage (EE%) (Y1), the particle size (Y2), and zeta potential (Y3) as shown in Table I. Twenty-six emulsomal formulae were prepared according to the chosen Central Composite Design, and the composition of each formula is shown in Table I.

Preparation of Syringic Acid Loaded Emulsomes

Syringic acid-loaded emulsomes were prepared using thin film hydration technique. Accurately weighed amounts of each of syringic acid, phosphatidylcholine, solid lipid (Tilaurin or tripalmitin), and cholesterol were dissolved in 10 mL of methylene chloride/methanol mixture (2:1) and transferred to a round-bottom flask. The total lipid amount was fixed at 400 mg, with cholesterol added in an amount equal to that of phosphatidylcholine. A rotary evaporator was used for the complete evaporation of the solvent under reduced pressure for 1 h at 40℃ and 120 rpm. Final traces of solvent were removed under vacuum, overnight. The formed film was then hydrated using 10 mL of phosphate buffer saline (pH 6.8) at 40℃ and 120 rpm for one hour and then sonicated using water bath sonicator (Elma Schmidbauer, Germany) for 1 min to reduce its size. Afterward, it was stored at 4℃ [30].

Characterization of the Prepared Emulsomes

Determination of Entrapment Efficiency % and Drug Loading % The entrapment efficiency % was determined using the indirect method as that reported by Sawant *et al.*, 2016 [31], with slight modifications. The free unentrapped drug was separated by centrifugation at 15000 rpm for 30 min at 4˚C (Sigma 3–30 KS, Sigma Laborzentrifugen, Germany), followed by washing the precipitate twice using phosphate buffer saline (pH 6.8). The free unentrapped drug was diluted and measured spectrophotometrically at $\lambda_{max.}$ 261nm (Shimadzu UV-1800 240 V, Japan) against blank emulsomes.

The EE % was calculated using Eq. 1 [32].:

$$\text{Syringic acid EE\%} = 1 - (\text{free drug in supernatant} / \text{original drug added}) * 100 \quad (1)$$

The drug loading % was calculated using Eq. 2:

$$\text{Drug Loading \%} = (\text{weight of SA inemulsomes/total weight of emulsomes}) * 100 \quad (2)$$

Determination of the Particle Size, Polydispersity Index (PDI), and Zeta Potential The particle size, polydispersity index (PDI) and zeta potential for the prepared emulsomes were measured using the dynamic light scattering method. A zeta sizer (Malven Zeta sizer version 6.20 serial number: MAL 104 4595, Worcestershire, United Kingdom) was used to measure the zeta potential via electrophoretic light scattering at a fixed angle of 173°. Following a tenfold dilution of the samples with deionized water to avoid multi-scattering phenomena, all measurements were made in triplicate [33].

Optimization of Syringic Acid-loaded Emulsomes The optimized formula (O_1) was identified by the Design Expert software according to the predefined constraints summarized in Table I. Selection was achieved through a numerical desirability function designed to maximize encapsulation

Table I Independent Variables Levels and Their Dependant Variables, Together With the Formulae and Their Composition, Using the Central Composite Design

Independent variables		**Levels of independent variables**				
	-α	**−1**	**0**	**+1**	**+α**	
X_1: SL: PC	0.5:1	0.866:1	1.75:1	2.633:1	3:1	
X_2: Drug amount (mg)	5	7.196	12.5	17.803	20	
X_3: Type of solid lipid		Tripalmitin		Trilaurin		
Dependent variable			**Desirability Constraints**			
	Y_1- Entrapment Efficiency (EE) (%)		Maximize			
	Y_2- Particle size (nm) (PS)		Minimize			
	Y_3- Zeta potential (mV) (ZP)		Maximize			
Formula code	**Independent variables level in their actual values**			**Dependent variables**		
	X_1	**X_2**	**X_3**	**Y_1**	**Y_2**	**Y_3**
F1	1.75:1	12.5	Tripalmitin	59.60 ± 0.92	375.80 ± 2.45	−52.00 ± 1.76
F2	1.75:1	5	Tripalmitin	32.12 ± 0.22	325.96 ± 2.78	−56.60 ± 1.89
F3	1.75:1	12.5	Tripalmitin	61.28 ± 0.51	337.34 ± 1.99	−52.60 ± 1.56
F4	1.75:1	12.5	Tripalmitin	57.24 ± 0.67	328.97 ± 2.12	−52.00 ± 1.76
F5	2.633:1	17.803	Tripalmitin	54.60 ± 0.65	285.10 ± 1.98	−55.1 ± 1.22
F6	0.866:1	17.803	Trilaurin	39.00 ± 0.22	221.60 ± 1.56	−52.00 ± 1.34
F7	1.75:1	20	Tripalmitin	48.49 ± 0.43	328.50 ± 2.56	−46.20 ± 1.54
F8	1.75:1	12.5	Trilaurin	40.07 ± 0.38	225.00 ± 1.98	−36.00 ± 1.33
F9	1.75:1	12.5	Trilaurin	42.00 ± 0.38	235.00 ± 1.77	−28.00 ± 1.21
F10	1.75:1	12.5	Tripalmitin	63.30 ± 0.56	330.18 ± 1.23	−51.10 ± 1.45
F11	3:1	12.5	Trilaurin	45.00 ± 0.34	177.00 ± 1.70	−35.00 ± 1.31
F12	1.75:1	12.5	Tripalmitin	62.96 ± 0.54	330.52 ± 1.34	−50.30 ± 1.45
F13	1.75:1	12.5	Trilaurin	44.00 ± 0.33	240.00 ± 2.09	−40.00 ± 1.45
F14	0.866:1	7.196	Trilaurin	28.11 ± 0.28	259.40 ± 1.89	−46.00 ± 1.41
F15	3:1	12.5	Tripalmitin	30.50 ± 0.31	286.60 ± 1.74	−57.90 ± 1.54
F16	0.866:1	7.196	Tripalmitin	29.79 ± 0.32	216.77 ± 1.25	−55.50 ± 1.51
F17	2.633:1	17.803	Trilaurin	30.00 ± 0.23	208.90 ± 1.67	−33.00 ± 1.34
F18	1.75:1	12.5	Trilaurin	41.00 ± 0.32	240.00 ± 1.37	−42.00 ± 1.38
F19	0.5:1	12.5	Trilaurin	35.84 ± 0.39	239.10 ± 1.33	−46.00 ± 1.41
F20	0.866:1	17.803	Tripalmitin	27.51 ± 0.25	257.50 ± 1.78	−48.30 ± 1.45
F21	2.633:1	7.196	Trilaurin	61.00 ± 0.45	176.30 ± 1.22	−35.00 ± 1.32
F22	2.633:1	7.196	Tripalmitin	24.52 ± 0.23	375.80 ± 2.65	−58.40 ± 1.45
F23	1.75:1	20	Trilaurin	36.8- ± 0.33	238.50 ± 2.09	−42.00 ± 1.41
F24	1.75:1	12.5	Trilaurin	42.00 ± 0.39	235.00 ± 2.53	−44.00 ± 1.31
F25	0.5:1	12.5	Tripalmitin	27.28 ± 0.25	205.40 ± 1.21	−50.70 ± 1.51
F26	1.75:1	5	Trilaurin	40.00 ± 0.32	217.70 ± 1.78	−41.00 ± 1.41

efficiency (EE%), minimize particle size (PS), and maximize zeta potential (ZP). The resulting optimized formulation (O_1) was subsequently prepared and experimentally evaluated to validate the accuracy of the optimization model.

Fourier Transform Infrared Spectroscopy (FTIR) Fourier transform infrared (FTIR) spectra of syringic acid, blank emulsomes, and the optimized emulsomes (O_1) were obtained using an FTIR spectrophotometer (JASCO FTIR-8400, Japan). Samples were prepared by mixing with dry potassium bromide, and spectra were recorded over the range of 4000–400 cm^{-1} at a resolution of 2 cm^{-1} (32).

Transmission Electron Microscopy (TEM) A drop of the optimized formulation (O_1) was deposited onto a carbon-coated copper grid and negatively stained with 1% (w/v) phosphotungstic acid to enhance contrast. Excess stain was removed using filter paper, and the grid was gently rinsed with distilled water and air-dried at room temperature. The sample was examined by transmission electron microscopy (TEM;

JEM-1230, JEOL, Tokyo, Japan) operated at an accelerating voltage of 200 kV and a magnification of × 25,000 to assess particle morphology [30].

***In-vitro* Drug Release Studies** To evaluate the *in-vitro* drug release of SA, a dialysis bag method was used. First, the dialysis membrane, which has a molecular weight cut-off of 12,000–14,000 Da, was soaked in the release medium overnight after being thoroughly cleaned with boiling water. The dialysis bags were then filled with a known volume of each optimized formula (O_1) and SA suspension (equivalent to 3 mg drug) (Standard SA) and were placed in containers with 100 mL of phosphate buffer saline (pH 6.8) [34] to simulate intestinal conditions, since the developed emulsomes are intended for oral administration and are expected to be absorbed mainly from the small intestine prior to entering systemic circulation.

The containers were incubated at 37 °C and 100 rpm in a thermostatically controlled shaker (incubator shaker, ZHWY-2102C, China). At specific time points over 24 h (0.5, 1, 2, 4, 6, 8, and 24 h), a volume of 2 mL from the samples were removed and immediately replaced with fresh dissolution medium. The samples were then filtered and analysed for SA spectrophotometrically at predetermined λ_{max} 261 nm [35]. The percentage of cumulative syringic acid release at each time interval was calculated using Eq. 3.

$$\%\ Cumulative\ release = (Amount\ of\ syringic\ acid\ in\ the\ medium / Original\ amount\ of\ syringic\ acid) \times 100 \quad (3)$$

The drug release profile was analysed using five mathematical models: zero-order, first-order, Korsmeyer–Peppas, Weibull, and Hixson–Crowell, employing KinetDS 3.0® software for the calculations [36].

Stability Studies

Stability studies were conducted according to ICH guidelines to ensure the stability of the optimized formula (O_1). Samples were stored for three months at 4 °C and 55–60% relative humidity. Following this time, the samples were visually examined and essential metrics such as particle size, zeta potential, entrapment efficiency percentage, and polydispersity index (PDI) were evaluated [30].

Pharmacokinetics Study

***In-vivo* Pharmacokinetics Study** The *in-vivo* pharmacokinetics study was conducted on 24 rats (each with an average weight of 0.25 kg) divided into two groups ($n = 12$). The first group (syringic acid) received standard syringic acid, and the second group (O_1) received the optimized formula. All groups were allowed to drink free water during the 12-h fasting. SA was administered to the syringic acid group at a dose of 6 mg/kg, orally, prepared as a suspension in water (standard SA). The O_1 group received a corresponding dose (6 mg/kg) of the O_1 formulation orally. Following oral administration, blood samples were taken from the retro-orbital plexus at 10, 30, 60, 90, 120, 180, 240, 300, and 1440 min in heparinized tubes. They were then centrifuged at 13,000 × g for 10 min at 4°C. The resultant plasma samples were kept at −80°C until HPLC analysis. The pharmacokinetic parameters were ascertained by non-compartmental analysis using Kinetica™ 2000 software (version 4.4.1, Thermo Electron Corporation, USA) [37, 38].

Chromatographic System and Conditions A binary solvent supply pump, autosampler, and photodiode array detector were all part of the Waters 2690 Alliance HPLC system (Waters, UK). Kinetex C18 (4.6 mm ID × 100 mm L, particle size 5 µm, Phenomenex, USA) was the stationary phase utilized. With a UV detector set at 290 nm and an injection volume of 10 µL, a mobile phase comprising 20% methanol and 80% acetic acid (0.1%) was supplied at a flow rate of 0.8 mL/min at room temperature.

Standard Working Solutions Standard working solution of syringic acid was prepared in the mobile phase to obtain concentrations of (1 mg/mL). For internal standard (IS), working solution was prepared in the same solvent (500 µg/mL).

Calibration Curves and Quality Control Samples 100 µL of each of the working standard solutions for SA and IS were added to 300 µL of rat plasma. The range of 50–500 µg/mL was used to prepare the plasma samples. Low (LQC), medium (MQC), and high (HQC) quality control samples were created in blank plasma at concentrations of 100, 250, and 400 µg/mL. The chromatograms were recorded after each sample was introduced into the HPLC system. Plotting the relative peak area (area of SA/area of IS (10 µg/mL)) against the corresponding concentration resulted in the calibration curve for each medication, from which the regression equations were computed.

Sample Preparation One hundred µL of the internal standard working standard solutions were added to 400 µL of rat plasma. To precipitate the proteins, 500 µL of extracting solvent (1% formic acid in methanol) was added right away, and the mixture was vigorously vortexed for two minutes. For ten minutes, the mixture was centrifuged at 10,000 rpm.

The clear supernatant was carefully transferred to a Wassermann tube, heated to 60 °C to concentrate it, and then reconstituted with mobile phase. The chromatogram was then recorded after 10 µL of the supernatant was put into the HPLC apparatus. The sample's concentration was calculated by substitution in the computed regression equation.

Method Validation Method validation was carried out according to FDA guidance for industry and bioanalytical method validation as listed in Supplementary material Table I SM.

Statistical Analysis

Design-Expert software (Version 13, Stat-Ease Inc., Minneapolis, MN) was used to statistically analyse the optimization data with linear regression and ANOVA. The analysis included comparing the coefficient of variation (CV), R^2, adjusted R^2, and predicted R^2 values. A *p-value* of less than 0.05 was considered statistically significant.

The *in-vivo* pharmacokinetics and stability data are presented as mean ± SEM. A one-way ANOVA was used to assess statistical differences between the experimental groups.

Physiologically Based Pharmacokinetic (PBPK) Model Building

Individual and Population Building Block (SA Monotherapy) PK-Sim® (v.12.0) software from Open Systems Pharmacology is a user-friendly software that simplifies whole-body physiologically based pharmacokinetic (PBPK) modelling, making it accessible to non-experts [39]. Using its pre-built components (Table II SM), a PBPK model was developed for syringic acid, a small acidic compound [9]. The model was initially built for an individual typical rat with an average weight of 0.25 kg and then scaled up to a virtual population of six rats. Key features of the model include: the model assumes that the distribution of syringic acid is limited by its permeability, a default assumption in PK-Sim for small molecules. The Rodgers and Rowland method was used to predict partition coefficients, while the Charge dependent Schmitt normalized to PK-Sim method was employed for cellular permeabilities, both of which are crucial for modelling an ionizable compound like syringic acid [40]. Furthermore, the model uses total hepatic clearance rather than individual enzymatic clearance values. The model is based on an immediate-release formulation of syringic acid. The overall modelling approach mirrors a case study published by Gandevia *et al*. (2023) [40], confirming a standard, established methodology.

Compound Parameters After being absorbed, syringic acid binds approximately to 38.6% with albumin and follows non-linear binding kinetics [41]. It is primarily metabolized by the liver via phase II conjugation and phase I oxidative/demethylation [42]. Metabolites formed from enzymes such as UGTs (UGT1A1, 1A9, and 2B7) and CYP450 isoenzymes (CYP1A2, 2C9 and 2D6) [41] are eliminated from the body via urine [43]. The compound parameters were Log $P = 1.04$, Molecular weight (g/moL) = 198.17 [41], Solubility at 25°C (mg/mL) = 1, and pKa (acid) = 4.43. Total clearance (mL/min/kg) = 7.21 [41]. The emulsomal formulation was incorporated into the PBPK model as an oral modified-release formulation, rather than explicitly modelling nanoparticle disposition. Specifically, the formulation was represented by adjusting dissolution/release kinetics based on *in-vitro* release data, absorption was modelled using the standard intestinal permeability framework in PK-Sim®. No explicit nanoparticle transport mechanisms (e.g., lymphatic uptake or carrier-mediated BBB transport) were assumed.

PBPK Model Building and Validation Blood, plasma, interstitial fluid (which represents the CSF), and intracellular compartments were the four default sub compartments used to simulate the brain. Through venous and arterial blood compartments, these sub compartments were connected to the whole PBPK model. PK-Sim maintained the default values for brain blood flow, volume, and weight [44].

The developed model was validated by comparison with the plasma pharmacokinetic study. Simulations were conducted using an oral dose of 6 mg/kg of syringic acid administered once daily. The predicted model data were compared to observed experimental data, focusing on key pharmacokinetic parameters such as maximum concentration (C_{max}) and the Area Under the Curve (AUC). Observed-to-predicted (obs/pred) ratios were calculated to determine fold error, and predictions were deemed acceptable if the ratios fell within the two-fold error range (0.5–2) [40].

Results and Discussion

Authentication of Syringic Acid

After several chromatographic isolation procedures, an off-white amorphous powder was obtained, having a melting point of 206 °C and was soluble in methanol. This compound had a retardation factor (R_f) value of 0.69 on TLC plates when eluted with a solvent composed of [dichloromethane—methanol (90:10 v/v)]. The compound appeared as an intense violet spot on paper chromatography under short UV light (254nm) having R_f value of 0.74 when developed using n-butanol – acetic acid – water (4:1:5) (upper phase) solvent system respectively. The spot gave a bluish violet color when sprayed with ferric chloride. For

further identification of the compound, its UV absorption spectrum exhibited two peaks at λ_{max} (methanol) 222 nm and 275 nm using UV spectrophotometer (Shimadzu UV-1800 240 V, Japan). These data were consistent with those of SA; thus, its identification was furthermore confirmed by co-chromatography with authentic SA (Sigma Aldrich) on paper chromatography using n-butanol – acetic acid – water (4:1:5) (upper phase) solvent system. Thus, the compound could be identified as 4-Hydroxy-3,5-dimethoxybenzoic acid (Syringic acid) ($C_9H_{10}O_5$).

Preparation of Syringic Acid Loaded Emulsomes

Emulsomes containing phosphatidylcholine and either tripalmitin or trilaurin solid lipids were prepared using the thin film hydration technique [45]. The solid lipid matrix enhances lipophilicity, thereby providing greater probable space for the entrapment of hydrophobic drugs [30, 46]. Tripalmitin was used at it is considered a suitable lipid for emulsomal cores due to its long saturated palmitic acid chains (C16) and high melting point (44.7–67.4°C), which enable the formation of a stable, well-organized matrix capable of incorporating larger amounts of lipophilic drug molecules. Trilaurin, a medium-chain triglyceride consisting of three lauric acid (C12) units, was also selected because it is considered a favourable candidate, as its remains solid at room temperature (25°C), exhibiting a melting point of 46.5°C [47].

Statistical Analysis Using Central Composite Design

A Central Composite Design was used to study the effects of the formulation variables, namely solid lipid to phosphatidyl choline ratio (SL: PC) (X_1), drug amount (X_2), and type of solid lipid (X_3), on the EE% (Y_1), PS (Y_2), and ZP (Y_3). The Central Composite Design (CCD) was selected as the framework for the response surface methodology owing to its robust statistical efficiency and flexibility. This design structure allows for the creation of orthogonal blocks, which facilitate the independent estimation of model parameters and block effects while minimizing variability in the regression coefficients. Furthermore, CCD provides a powerful means of modelling complex relationships by enabling the construction of quadratic response surfaces that accurately describe the interaction between experimental variables and the measured responses [38]. A notable advantage of this design lies in its efficiency, as it requires a relatively smaller number of experimental trials to attain the same degree of model precision and complexity, making it particularly advantageous when dealing with multiple influencing factors or higher-order interactions [48, 49].

The final design consists of 26 trial runs, and Table I shows the EE%, PS, and ZP results. The optimized formula was chosen to have a minimum particle size, maximum zeta potential, and maximum EE%. The design showed a reduced cubic model for all the measured responses, as can be represented in Table II and Fig. 1. The fitted models had a high correlation coefficient R^2, an adjusted R^2 in a reasonable agreement with the predicted R^2, and adequate precision values of (0.9604, 0.9453, 0.8303, 18.982, for EE %, 0.9659, 0.9392, 0.8705, 19.121 for particle size, and 0.8861, 0.7966, 0.7131, 10.139 for the zeta potential, respectively). This suggests that the design space can be navigated using the models for every response. The significant terms were found using the ANOVA test. Terms in the model were deemed statistically significant if their *p-value* was less than 0.05.

Effect of Independent Variables on EE%

The entrapment efficiency % of the formulated syringic acid-loaded emulsomes ranged from $24.52\% \pm 0.23\%$ to $63.30 \pm 0.56\%$. The drug loading % ranged from $0.78 \pm 0.03\%$ to $4.46 \pm 0.26\%$. The effect of independent variables on EE% is shown by Eq. (4):

$$EE\% = +51.35 + 3.95X_1 + 1.64X_2 - 9.53X_3 - 4.72X_2X_3 - 8.93X_1^2 - 6.04X_2^2 - 9.28X_1X_2X_3 + 7.72X_1^2X_3 + 4.37X_2^2X_3 \quad (4)$$

$$EE\ \%\ using\ tripalmitin = -43.91 + 54.36X_1 + 7.43X_2 + 1.73X_1X_2 - 20.63X_1^2 - 0.37X_2^2 \quad (4a)$$

$$EE\ \%\ using\ trilaurin = -20.86 + 36.13X_1 + 4.82X_2 - 2.23X_1X_2 - 0.85X_1^2 - 0.06X_2^2 \quad (4b)$$

Table II illustrates that the three studied independent variables significantly influenced the entrapment efficiency (EE%), as shown by the *p-value* less than 0.05.

As can be deduced from Eq. 4, an increase in the SL: PC ratio (X_1) and drug amount (X_2), resulted in an increase in EE% as evidenced by their positive coefficients. The

Table II ANOVA for the Measured Responses

Source	Y_1 = EE%					Y_2 = PS					Y_3 = ZP				
	Sum of Squares	DF	Mean Square	F-Value	*p*-value	Sum of Squares	DF	Mean Square	F-Value	*p*-value	Sum of Squares	DF	Mean Square	F-Value	*p*-value
Model	3787.289	11	344.299	40.312	< 0.0001		11	7543.517	36.089	< 0.0001		11	139.509	9.901	< 0.0001
X_1: SL: PC	249.782	1	249.782	29.246	< 0.0001	867.913	1	867.913	4.152	0.061	41.197	1	41.197	2.924	0.109
X_2: Drug amount	43.281	1	43.281	5.068	0.041	30.698	1	30.698	0.147	0.707	24.487	1	24.487	1.738	0.209
X_3: Type of SL	908.400	1	908.400	106.360	< 0.0001	27858.340	1	27858.34	133.277	< 0.0001	462.400	1	462.400	32.816	< 0.0001
X_1X_2	11.353	1	11.353	1.329	0.268	465.583	1	465.583	2.227	0.158	2.101	1	2.101	0.149	0.705
X_1X_3	6.852	1	6.852	0.802	0.386	14706.825	1	14706.825	70.359	< 0.0001	267.639	1	267.639	18.994	0.001
X_2X_3	357.079	1	357.079	41.809	< 0.0001	311.465	1	311.465	1.490	0.242	58.607	1	58.607	4.159	0.061
X_1^2	979.806	1	979.806	114.720	< 0.0001	13302.752	1	13302.75	63.642	< 0.0001	33.291	1	33.291	2.363	0.147
X_2^2	508.095	1	508.095	59.490	< 0.0001	436.537	1	436.537	2.088	0.170	15.985	1	15.985	1.134	0.305
$X_1X_2X_3$	689.133	1	689.133	80.687	< 0.0001	5091.919	1	5091.919	24.360	0.000	17.701	1	17.701	1.256	0.281
$X_1^2X_3$	830.108	1	830.108	97.193	< 0.0001	4051.765	1	4051.765	19.384	0.001	0.411	1	0.411	0.029	0.867
$X_2^2X_3$	265.149	1	265.149	31.045	< 0.0001	43.597	1	43.597	0.209	0.655	8.974	1	8.974	0.637	0.438
Residual	119.571	14	8.541			2926.362	14	209.026			197.267	14	14.090		
Lack of Fit	85.789	6	14.298	3.386	0.057	1181.262	6	196.877	0.903	0.537	34.007	6	5.668	0.278	0.932
Pure Error	33.783	8	4.223			1745.100	8	218.138			163.260	8	20.408		
Cor Total	3906.860	25				85905.049	25				1731.867	25			

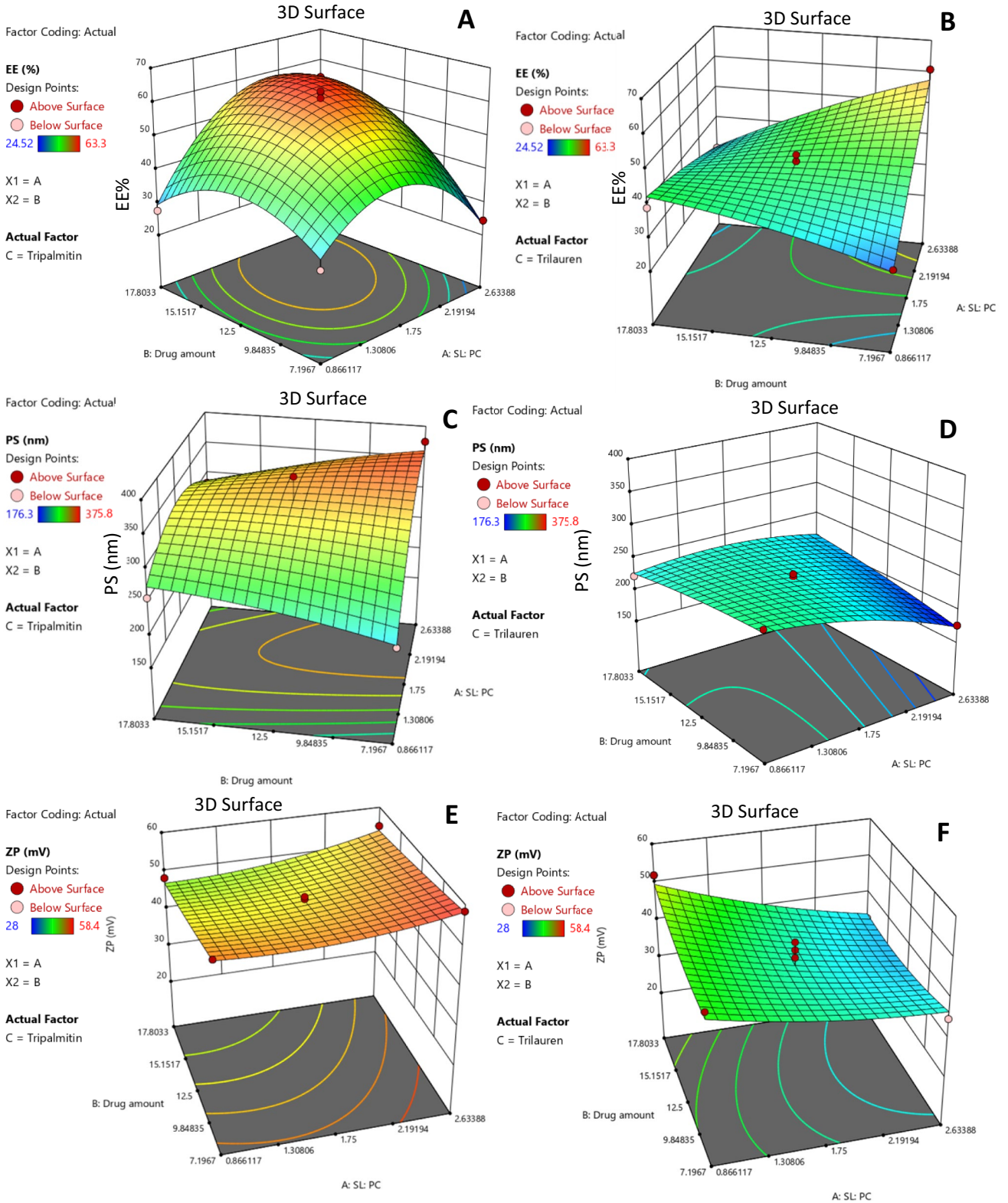

Fig. 1 3D response surface plot showing the effect of the SL:PC (X_1) and the drug amount (X_2) on (**A**) the EE% using Tripalmitin, (**B**) the EE% using Trilaurin, (**C**) the particle size using Tripalmitin (**D**) the particle size using Trilaurin, (**E**) the zeta potential using Tripalmitin and (**F**) the zeta potential using Trilaurin

use of tripalmitin (X_3) also contributes to enhanced EE%. The increase in EE% upon the increase in the solid lipid to phospholipid ratio (X_1) could be due to several interconnected physical and chemical mechanisms. Structurally, the solid lipid forms the lipophilic core of the emulsomes, is expectedly serving as the primary reservoir for hydrophobic molecular payloads. Syringic acid possesses a dimethoxy-substituted aromatic ring that imparts moderate lipophilicity and enhances its affinity for lipidic environments. Consequently, the drug is expected to partition into the solid lipid matrix and associate with the phospholipid interface through hydrophobic interactions and van der Waals forces. Increasing the solid lipid to phosphatidyl choline ratio expands this core volume, thereby offering probable greater accommodation and retention capacity for the drug molecules within the lipid matrix [50]. Moreover, when the lipid content increases, more drug partitions into the lipid phase, shifting the equilibrium away from the aqueous phase. This is especially important during the emulsification process when drug molecules can distribute between aqueous and lipid phases. In addition, a higher lipid content leads to a denser and more structured core, reducing drug diffusion and leakage during preparation and storage [51]. On the other hand, the increase in the drug amount (X_2) resulted in an increase in the likelihood of drug molecules interacting with the lipid core, leading to greater entrapment. This is particularly evident with lipophilic drugs, which have a higher affinity for the lipid phase. For instance, a study on bifonazole emulsomes demonstrated that increasing the drug percentage led to higher EE%, attributed to more drug being available for encapsulation [52].

Finally, the type of solid lipid used in emulsomes formulation can significantly impact EE%. The better EE% upon the use of tripalmitin as the lipid core could be due to the longer fatty acid chain of tripalmitin (C16), as compared to trilaurin (C12) which resulted in higher drug encapsulation [47, 52].

The 3D response surface plots illustrated the interactive effects of the formulation variables on EE% for both tripalmitin- (Fig. 1A, Eq. 4a) and trilaurin-based emulsomes (Fig. 1B, Eq. 4b). For the tripalmitin formulation, EE% increased with higher SL:PC ratios (X1) up to an inflection point of approximately 1.75:1, beyond which further lipid addition resulted in a gradual decline in encapsulation [22, 46]. This biphasic behaviour reflects the strong negative quadratic coefficient for the lipid ratio ($X_1^2 = -20.63$) (Eq. 4a), indicating that an optimal SL:PC ratio exists for achieving specific EE% targets. Similarly, increasing the initial drug payload (X2) initially improved EE% due to enhanced mass availability, but excessive drug feeding led to matrix saturation, resulting in drug expulsion, leakage, or phase separation, as reflected by the negative quadratic coefficient ($X_1^2 = -0.37$) [47]. The pronounced curvature of the response surface in Fig. 1A signifies a nonlinear interaction, indicating that maximum EE% is achieved at an intermediate SL:PC ratio combined with a moderate drug payload. In contrast, the response surface for the trilaurin systems (Fig. 1B) exhibited a noticeably less pronounced curvature; this indicates that tripalmitin-based emulsomes afford a wider acceptable formulation space regarding the SL:PC ratio, thereby offering superior manufacturing and processing flexibility.

Effect of Independent Variables on Particle Size

The formulated syringic acid-loaded emulsomes particle size ranged from 176.30 ± 1.22 to 375.80 ± 2.45 nm. The impact of independent variables on particle size is presented in Eq. 5.

$$PS = +287.78 + 7.37X_1 - 1.39X_2 - 52.78X_3 - 30.32X_1X_3 - 30.92X_1^2 + 25.23X_1X_2X_3 + 17.07X_1^2X_3 + 1.77X_2^2X \quad (5)$$

$$PS\ using\ tripalmitin = -102.78 + 345.23X_1 + 17.73X_2 - 7.01X_1X_2 - 61.42X_1^2 - 0.26X_2^2 \quad (5a)$$

$$PS\ using\ trilaurin = +279.84 - 10.83X_1 - 2.59X_2 + 3.75X_1X_2 - 17.74X_1^2 - 0.14X_2^2 \quad (5b)$$

Table II illustrates that only the type of solid lipid significantly influenced the particle size with *p-value* less than 0.05, with a quadratic SL: PC ratio significant effect. The model was found to be reduced cubic model. As could be observed from Eq. 4, the utilization of tripalmitin as the lipid core material yielded a more pronounced increase in particle size compared to trilaurin, a phenomenon driven by several interconnected physicochemical mechanisms. Tripalmitin is composed of longer saturated fatty acid chains (C16, palmitic acid) relative to the shorter chains of trilaurin (C12, lauric acid). These elongated hydrocarbon chains inherently amplify intermolecular van der Waals interactions, elevating matrix hydrophobicity while restricting molecular mobility, which in turn leads to more aggregated lipid cores during preparation and larger final particles [25, 53]. Furthermore,

this acyl chain length fundamentally dictates the crystallization kinetics and phase behaviour of the lipid core; longer-chain triglycerides like tripalmitin exhibit higher melting points and a stronger propensity to crystallize more readily during cooling, generating highly rigid, less flexible crystalline structures. This structural rigidity increases matrix viscosity during emulsification and resists mechanical shear, thereby hindering the efficient breakdown of the droplets into smaller nanoparticles and favouring larger particle sizes compared to those formed with shorter-chain trilaurin matrices [54].

The interactive effects of the formulation variables on particle size are illustrated in the 3D response surface plots for tripalmitin- (Fig. 1C, Eq. 5a) and trilaurin-based emulsomes (Fig. 1D, Eq. 5b). For the tripalmitin system, particle size increased alongside the SL:PC ratio (X_1) up to an inflection point of approximately 1.75:1, beyond which further lipid addition caused a gradual decline in vesicle size. This biphasic behaviour is corroborated by the pronounced negative quadratic coefficient for the lipid ratio X_1^2(– 61.42). Mechanistically, low SL:PC ratios feature higher phospholipid fractions that enhance emulsification efficiency by improving interfacial coverage and reducing interfacial tension, yielding smaller particles [55, 56]. Initial increase in the SL:PC ratio could expand the lipid core, enhance drug encapsulation, and increase system viscosity, which favors the formation of larger particles or promotes coalescence during emulsification [57]. However, exceeding the optimal matrix threshold could shift the balance between interfacial stabilization and bilayer thickness, reducing particle size. Conversely, increasing the initial drug payload (X_2) led to a corresponding enlargement of particle size, which can be attributed to the disruption of lipid packing or elevated internal osmotic pressure that induces swelling of the vesicular core [58]. Much like the trends observed for encapsulation, the trilaurin systems (Fig. 1D) displayed a flatter, less pronounced curvature, indicating that the shorter-chain matrix affords a broader acceptable formulation window and superior manufacturing flexibility.

Impact of Independent Variables on Zeta Potential

One important factor influencing the stability of colloidal dispersion is the zeta potential. Because of the electrical repulsion between particles, particles are typically dispersed steadily when the absolute value of the zeta potential is more than ± 30 mV [59]. The zeta potential of the formulated syringic acid-loaded emulsomes ranged from −28.00 ± 1.21 to −58.4 ± 1.45 mv. Because of the large absolute value of the zeta potential, which lowers the likelihood of coalescence, the created emulsomes were therefore anticipated to be physically stable [60]. The presence of anionic phospholipids in the outer bilayer of the emulsomes is responsible for their reported negative zeta potential [61].

The impact of independent variables on zeta potential is shown by Eq. (6).

$$ZP = +44.80 - 1.60X_1 - 1.24X_2 - 6.80X_3 - 4.09X_1X_3 \quad (6)$$

$$ZP\ using\ Triplamitin = +66.88 - 7.49X_1 - 1.19X_2 + 0.20X_1X_2 + 2.2X1^2 + 0.01X2^2 \quad (6a)$$

$$ZP\ using\ Trilaurin = +54.15 - 7.27X_1 - 0.79X_2 - 0.42X_1X_2 + 1.76X1^2 + 0.06X2^2 \quad (6b)$$

As shown in Table II, the type of solid lipid was the only factor that significantly affected zeta potential (ZP) ($p < 0.05$), and the response was best described by a reduced cubic model. According to Eq. 6, emulsomes formulated with tripalmitin exhibited significantly higher ZP values than those prepared with trilaurin. This difference may be attributed to variations in fatty acid chain length, lipid crystallinity, and the resulting organization of the interfacial phospholipid layer.

The interactive effects of the formulation variables on ZP are presented in the three-dimensional response surface plots for tripalmitin- (Fig. 1E, Eq. 6a) and trilaurin-based emulsomes (Fig. 1F, Eq. 6b). The relatively flat response surfaces indicate that changes in the SL ratio (X1) and drug amount (X2) exerted minimal influence on ZP. Consistent with these observations, ANOVA results confirmed that the solid lipid type (X3) was the sole independent variable significantly affecting ZP ($p < 0.05$), while all other factors and interaction terms were statistically insignificant. These findings suggest that the surface electrical properties of the emulsomes were governed primarily by the nature of the lipid core.

The longer C16 hydrocarbon chains of tripalmitin favor the formation of highly ordered β-polymorphic crystals, resulting in a rigid lipid matrix that promotes tighter phospholipid packing and stronger anchoring of surfactant molecules at the particle interface [62]. This enhanced interfacial organization increases surface charge density, leading to significantly higher ZP values [63]. In contrast, the shorter C12 chains of trilaurin produce less ordered and more fluid crystalline structures, which weaken interfacial packing and surfactant anchoring, thereby reducing the surface charge density and yielding lower ZP values [14, 63].

Response Surface Optimization of SA Loaded Emulsomes

The optimum variables were chosen through optimization to create SA-loaded emulsomes with the highest zeta potential, the smallest particle size, and the highest EE%. Table III lists the desirability, predicted and observed responses, and the composition of the optimized SA-loaded emulsomes.

An optimized formula (O_1) was suggested by the Design expert software. It is composed of a ratio of solid lipid to phosphatidyl choline of 2.634:1, drug amount of 7.197 mg, and trilaurin as the solid lipid, with a desirability of 0.932. The optimized formula was prepared and characterized in terms of EE%, particle size, and zeta potential to calculate the % prediction error. As shown in Table III the EE % and the particle size and the zeta potential for the optimized formula were $61.92 \pm 0.09\%$, 190.02 ± 0.13 nm, and -36.31 ± 0.98 mv respectively. All responses had very low prediction errors (Table III), suggesting that this approach might be effectively used for optimization of SA-loaded emulsomes. Additionally, the optimized formulation exhibited a PDI of 0.21 ± 0.07, indicating a narrow particle size distribution and good formulation homogeneity.

Fourier Transform Infrared Spectroscopy (FTIR)

The FTIR spectra of syringic acid, blank emulsomes, and the optimized syringic acid-loaded emulsomes are shown in Fig. 2. Syringic acid exhibited characteristic absorption bands at 3371.57 cm^{-1}, corresponding to O–H stretching, and at 1697.36 cm^{-1}, attributed to C = O stretching of the carbonyl group. These characteristic peaks were absent in the FTIR spectrum of the blank emulsomes, confirming the absence of the drug in the unloaded formulation. Furthermore, the characteristic peaks of syringic acid at 3371.57 cm^{-1} (O–H stretching) and 1697.36 cm^{-1} (C = O stretching) were not observed in the spectrum of the optimized drug-loaded emulsomes. The disappearance of these characteristic bands suggests that syringic acid was successfully encapsulated within the emulsomal system and was molecularly dispersed within the lipid matrix rather than remaining in its crystalline form [64].

Transmission Electron Microscopy Analysis

The morphology of the emulsomes was examined using transmission electron microscopy (TEM), as presented in Fig. 3A. The TEM images demonstrated well-defined, spherical vesicles with no detectable aggregation, with a particle size of 190.02 ± 0.13 nm [37]. The vesicles appeared as discrete spherical particles encased by phospholipid bilayers, and the analysis further confirmed the presence of a distinct lipidic core enveloped by an outer phospholipid shell [24].

In-vitro Drug Release Analysis

The *in-vitro* release study was conducted in phosphate-buffered saline (pH 6.8) to simulate intestinal conditions, as the developed emulsomes are intended for oral administration and are expected to be absorbed primarily from the small intestine before entering systemic circulation.

The structural characteristics of emulsomes contribute significantly to their ability to sustain drug release. Their solid lipidic core mostly enables the efficient encapsulation of lipophilic drugs such as syringic acid, while the dense lipid matrix and the surrounding phospholipid bilayer act as diffusion barriers, retarding drug escape. As a result, drug release may occur gradually as the encapsulated molecules diffuse outward from the lipid core through the phospholipid bilayer, thereby generating a sustained release profile [65, 66] This mechanistic behaviour was clearly reflected

Table III The Optimized Values of the Variables With the Predicted and Observed Responses

Optimized Formula Composition	Response	Predicted value	Observed value	Prediction error%*	Desirability
X_1: SL: PC (2.634:1) X_2: Drug amount (mg) (7.197) X_3: Type of solid lipid (Trilaurin)	*EE (%)*	57.62	61.92 ± 0.09	7.46	0.932
	Particle size (nm)	173.733	190.02 ± 0.13	9.37	
	Zeta potential (mv)	−36.87	-36.31 ± 0.98	1.51	

*Prediction error = Predicted value – Observed value/Predicted value X 100

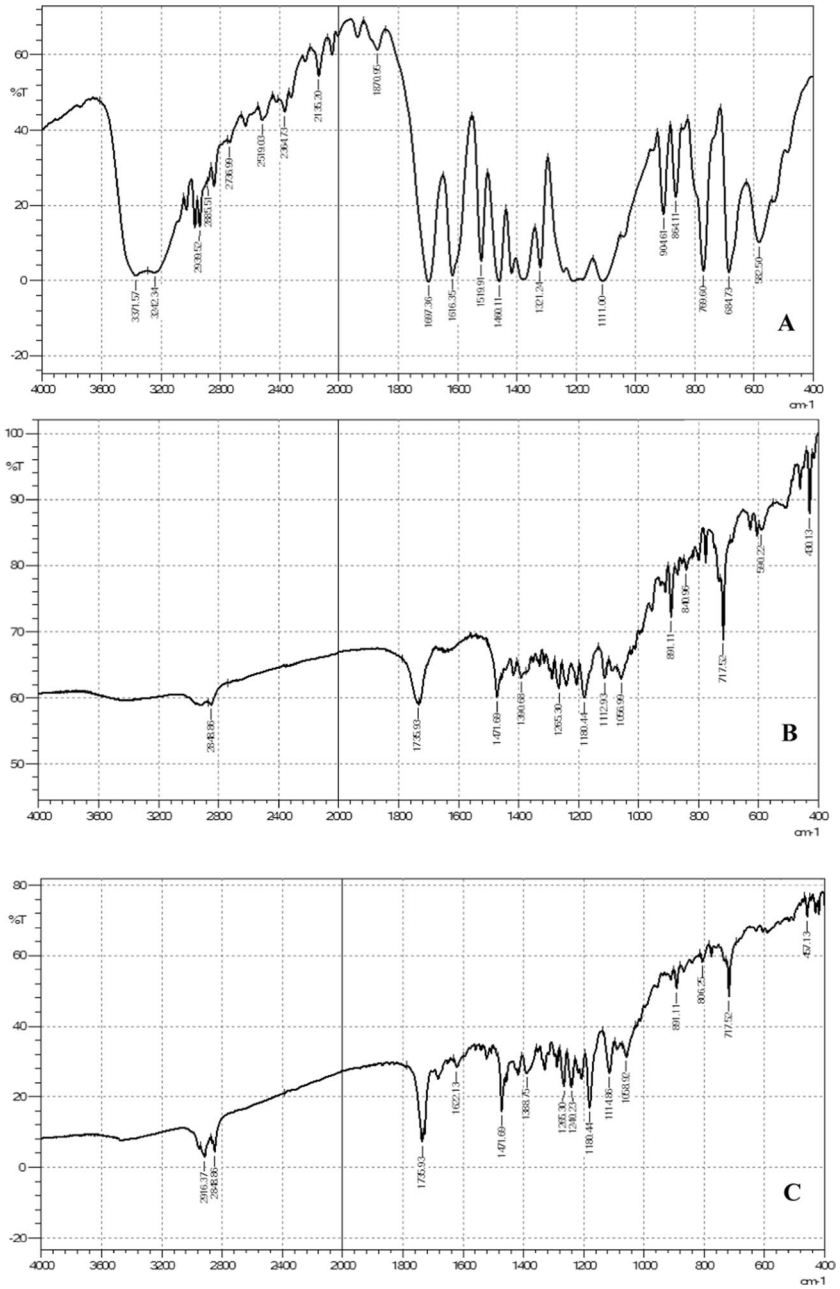

Fig. 2 FTIR spectra of **A**-Syringic acid **B**-Blank emulsomes **C**-Optimized emulsomes formula

in the present findings. The release profile of SA from the optimized emulsomal formulation demonstrated a distinct deviation from that of the free drug (Fig. 3B). The optimized formulation (O_1) exhibited a biphasic release pattern, with an initial burst of 15.38 ± 0.54% at 1 h and 37.26 ± 0.65% at 6 h, 50.82 ± 0.67% at 12 h, followed by a markedly sustained phase, reaching 92.50 ± 1.30% at 24 h. In contrast, free SA (Standard SA) reached 21.24 ± 0.57% at 1 h and 25.07 ± 0.97% at 6 h, 25.38 ± 0.24% at 12 h, and plateaued at only 25.20 ± 0.76% by the end of 24 h [67]. The initial burst release observed in the optimized formula is likely due to desorption of surface-associated drug molecules, whereas the sustained release phase is attributed to the gradual diffusion of SA from the inner core and the associated phospholipid bilayers [68–71]. The improved release performance of emulsomal formulations can also be explained by their nanoscale size and enlarged surface area, which enhance drug solubilization. Furthermore, the surface-active properties of amphiphilic lecithin, forming the outer shell layers, play a critical role in promoting drug release from the developed systems [26, 64, 71]. Overall, the results underscore the potential of emulsomes as a promising delivery system for improving the solubility of lipophilic drugs such as syringic acid while simultaneously achieving sustained release.

In-vitro release data were fitted to several kinetic models, including zero-order, first-order, second-order,

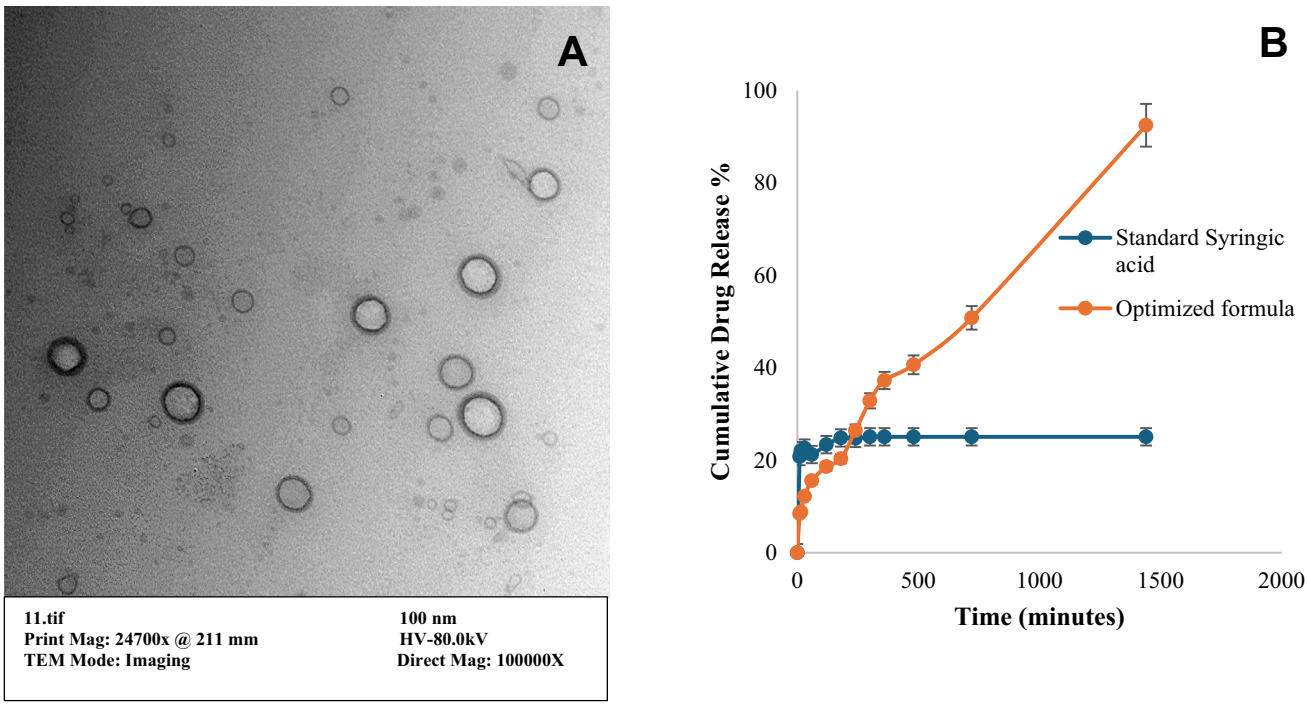

Fig. 3 **A**- TEM photos of the optimized formula **B**- *In-vitro* drug release of the optimized formula as compared to the standard Syringic acid

Korsmeyer–Peppas, and Weibull, yielding correlation coefficients (R^2) of 0.9762, 0.0768, 0.0403, 0.9967, and 0.9972, respectively. The Weibull model (with lag time) exhibited the highest correlation, indicating that it best describes the release behaviour of syringic acid from syringic acid-loaded optimized formula. The mass transport mechanism is postulated to be a sequential process involving SA diffusion through the lipid matrix to the particle surface, interfacial partitioning between the lipid core and the aqueous medium, and subsequent dissolution and dialytic transport. This complex behavior was mathematically validated by the Weibull shape parameter (ß). In this study, a value of ß < 0.75 confirmed that SA release from the emulsomes is predominantly governed by Fickian diffusion. From a clinical perspective, this prolonged and controlled release profile offers distinct advantages, including reduced dosing frequency, minimized systemic fluctuations, and mitigated adverse effects, which collectively enhance patient compliance and the therapeutic efficacy of orally administered SA [72].

Stability Studies

The physical stability of the optimized emulsomes was evaluated over three months at 4°C. Freshly prepared emulsomes (Time 0) exhibited a particle size of 190.02 ± 0.13 nm, a PDI of 0.21 ± 0.07 and a ZP of –36.3 ± 0.98 mV, and an encapsulation efficiency of –36.3 ± 0.98 mV%. After three months of storage at 4 °C, stability studies showed that the optimized emulsomes maintained its original colour and lacked any visible clumping. The encapsulation efficiency was 60.55 ± 1.11%, the particle size was 192.23 ± 1.07 nm, the PDI was 0.21 ± 0.07 and the zeta potential was – 35.55 ± 0.79 mV, which were all not statistically significant (results not shown) than when freshly prepared. These results demonstrate the excellent stability of the developed emulsomes when stored at 4 ◦C.

In-vivo Pharmacokinetics Study

HPLC Method Development and Optimization

One of the challenges in bioanalysis is the quantification of minute amounts in plasma and their effective extraction from the plasma matrix with acceptable recovery. For this elution, two C18 columns with different lengths (100 mm and 250 mm) were evaluated; the shorter one demonstrated a shorter runtime and an acceptable resolution between syringic acid and IS. A variety of mobile phase compositions, including various solvent ratios such as acetonitrile, methanol, phosphate, and acetate buffer, were investigated. Lastly, Kinetex C18 (4.6 mm ID × 100 mm L, particle size 5 µm, Phenomenex, USA) was utilized at UV detection at 290 nm with a mobile phase composition of 20% methanol and 80% acetic acid (0.1%). Sharp, symmetrically resolved peaks with good analyte sensitivity were visible in the chromatogram (Fig. 4A). The developed methods [73, 74] offers the benefit

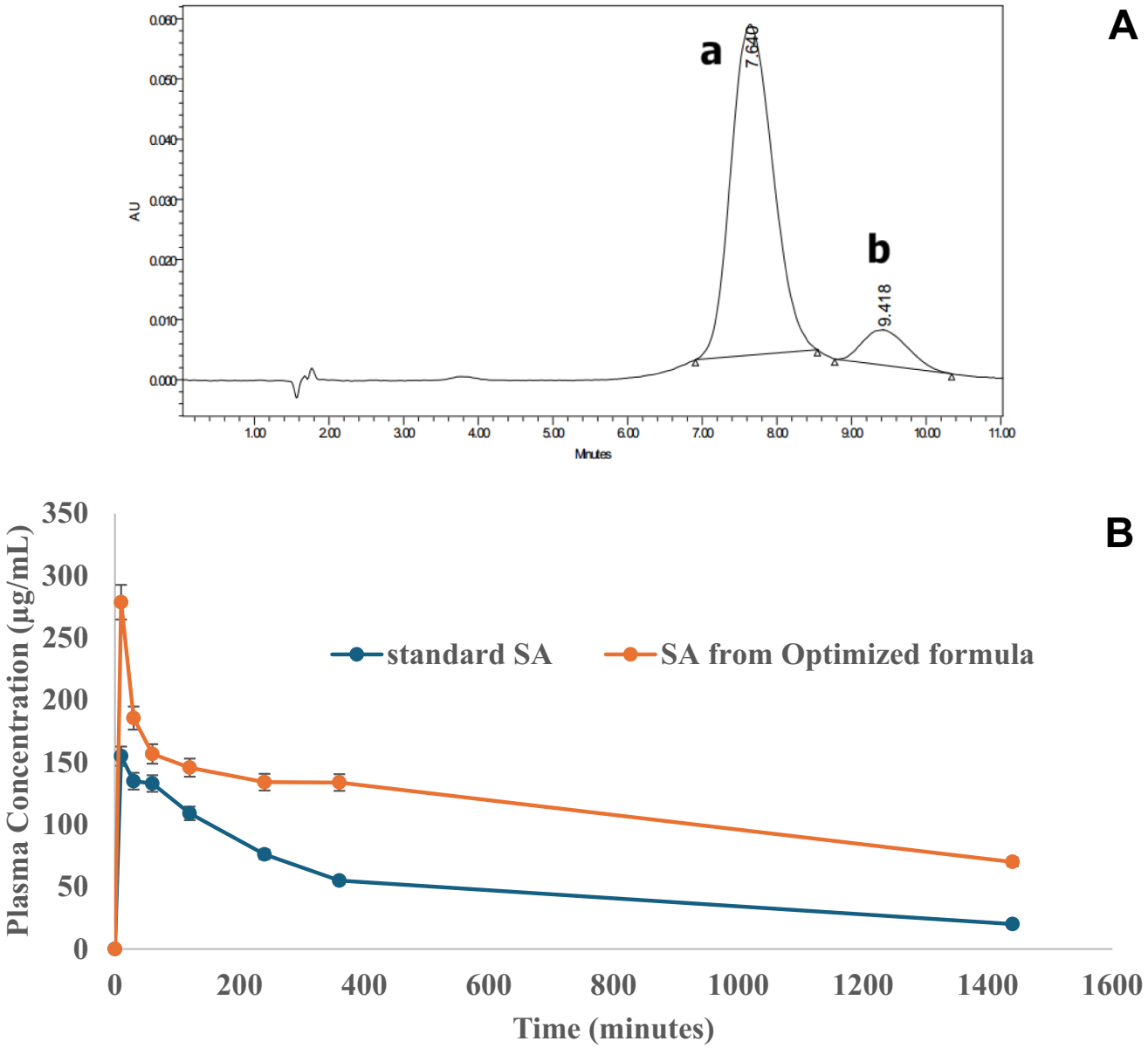

Fig. 4 **A**- HPLC chromatogram showing separated peaks of (**a**) syringic acid and (**b**) IS **B-** Mean plasma concentration–time curve of syringic after oral administration

of employing a more environmentally friendly mobile phase than the other documented techniques, which used a straightforward isocratic program with just 20% organic solvent for elution.

Validation Sheet and Extraction Procedure

Simple protein precipitation was used because it saves money and time by requiring modest sample size and using a little amount of organic solvents. According to Table I SM in the supplemental material, methanol demonstrated an adequate extraction recovery and matrix effect for syringic acid from plasma samples. The outcomes of the four stability studies were satisfactory. Table IV listed the validation sheet with linearity, LOD, LOQ, accuracy, and precision. To make the eluted peaks more symmetrical, formic acid was added. Table IV's system suitability parameters were computed using USP reference 4.

Pharmacokinetics Study Analysis

Rats were used to test and compare the oral bioavailability of SA from the optimized formula with that of SA. Table V summarizes the key pharmacokinetic parameters obtained.

Table IV System Suitability and Validation Parameters for the Proposed HPLC–UV Method

Parameters	HPLC	USP Reference values
Linearity (µg/mL)	5–500	
Correlation coefficient (r)	0.9990	
Slope	0.0656	
Intercept	−0.2036	
SD of residuals from line	0.3245	
LOD (µg/mL)	16.33	
LOQ (µg/mL)	49.47	
Accuracy (Recovery % ± SD)	98.87 ± 1.88	
Precision (Intraday)	98.11 ± 2.15	
Precision (Inter-day)	100.98 ± 2.44	
Extraction recovery RSD%	77.83	
Matrix effect	82.11	
t_R, min	7.64 ± 0.02	
Tailing factor (T)	1.05	T ≤ 2, T = 1 for symmetric peak
Capacity factor (K')	2.05	K' = 1–10 acceptable
Plates number (N)	3774	$N > 2000$
Height equivalent to theoretical plate (HETP)	0.05	The smaller the value, the higher the column efficiency
Experimental resolution (Rs)**	2.10	Rs ≥ 2

*Experimental Resolution between syringic acid and internal standard

Table V Pharmacokinetic Parameters of Standard SA and Syringic Acid From the Optimized Formula

Parameter	Standard SA (Plasma)	SA from Optimized Formula (Plasma)	Standard SA (Brain)	SA from Optimized Formula (Brain)
C_{max} (µg/mL) Observed	154.98 ± 3.21	278.73 ± 7.34[a]	37.40	45.36
C_{max} (µg/mL) Predicted	226.6	187.7		
	Observed/Predicted = 0.68	Observed/Predicted = 1.48		
T_{max} (min)	10 ± 0.05	10 ± 0.07		
AUC $_{0–24}$(µg.min/mL) Observed	74412.2 ± 19.22	163174 ± 77.76[a]	27621	29666
AUC $_{0–24}$(µg.min/mL) Predicted	132690	148200		
	Observed/Predicted = 0.56	Observed/Predicted = 1.10		
AUC $_{0-\infty}$ (µg.min/mL)	93389.7 ± 32.13	286683 ± 55.22[a]	31342.8	35900
AUMC $_{0–24}$ (µg.min^2/mL)	3.128 e^{+007} ± 201.11	8.937 e^{+007} ± 312.55[a]		
AUMC $_{0-\infty}$ (µg.min^2/mL)	7.680 e^{+007} ± 314.22	4.847e^{+008} ± 454.76[a]		
Mean residence time (min)	822.41 ± 9.22	1690.79 ± 17.75		

Cmax peak plasma concentration, Tmax time to reach peak plasma concentration, AUC 0–24 area under the plasma concentration–time curve from time 0 to 24 h, AUC 0–∞ area under the plasma concentration–time curve calculated by the linear trapezoidal rule from time 0 to infinity, AUMC0–24 area under the first moment curve from time 0 to 24 h, AUMC0–∞ area under the first moment curve from time 0 to infinity

[a]Significant difference from standard syringic acid group. Data is presented as mean ± SD

The mean plasma concentration time profiles of SA were constructed by plotting the average drug concentrations in rat plasma at the specified time points, as illustrated in the Fig. 4B. The optimized SA-loaded emulsomes achieved a C_{max} of 278.73 ± 7.34 µg/mL versus 154.98 ± 3.21 µg/mL for the standard SA (approximately 1.8 times higher). The higher C_{max} could be attributed to the lipid core structure of emulsomes that enables efficient encapsulation of SA. The solid lipid core enclosed within the phospholipid bilayer offers a stable matrix for hydrophobic drugs, thereby improving their solubility, and bioavailability [25]. The emulsomes remained in the plasma significantly longer (2 times longer), with a mean residence time of 1690.79 ± 17.75 min. versus 822.41 ± 9.22 min for the standard SA. This could be attributed to the size of emulsomes as it has been reported that nanoparticles of particle size less than 200 nm are known to

escape reticular endothelial system (RES) and hence have long blood circulation [75]. Moreover, the increased mean residence time of the emulsomes suggest an extended systemic retention, likely resulting from their sustained-release properties, which may translate into a longer duration of therapeutic action [76]. The optimized emulsomes showed a significantly greater AUC_{0-24} (163174 µg.min/mL) versus (74412.2 µg.min/mL) for standard SA. This resulted in a relative bioavailability of about 219% for the optimized formulation, suggesting a substantial increase in the drug's absorption into the bloodstream when delivered via emulsomes. The significant enhancement in the bioavailability of emulsomes can be attributed to their small size which markedly improve drug solubility and absorption by facilitating easier penetration across cellular membranes [77]. Furthermore, the presence of soya lecithin helps protect the encapsulated drug from the harsh gastric environment, premature metabolism and enzymatic degradation [25]. Moreover, emulsomes (structurally similar to chylomicrons) promote enhanced drug absorption across the intestinal mucosa as they are taken up via M cells in Peyer's patches and subsequently transported through the lymphatic pathway, effectively circumventing hepatic first-pass metabolism. As a result, higher systemic drug concentrations are achieved compared to conventional nano vesicular systems, which typically undergo significant hepatic metabolism prior to systemic circulation. This lymphatic transport mechanism contributes to superior transcellular movement and absorption, and thus higher bioavailability [23, 25, 78, 79]. These findings pave the way for future investigations involving more extensive preclinical studies to comprehensively assess the efficacy and safety of the developed SA-loaded emulsomes as a neuroprotective agent in many neurodegenerative diseases.

Figure 5A and B depict the plasma time-concentration profile for the simulated oral model with a standard administration protocol of 6 mg/kg. After that, the simulated and observed data were compared and verified [39].

The observed-to-predicted ratios for the mean values of individuals during model validation ranged from 0.68 to 1.48 for C_{max} and from 0.56 to 1.10 for AUC, as can be deduced from Table V. As depicted the ratios were well within acceptable two-fold variation. These ratios being close to 1 indicate a strong agreement between the observed experimental data and the model's predicted values [39].

The simulated PK profile was comparable with the experimental data, thus was used to simulate the brain pharmacokinetics as well. It is worth mentioning that the brain distribution results were PBPK-predicted only. The simulated C_{max} and AUC values indicate that the formulated syringic acid in emulsomes may improve the brain bioavailability of syringic acid compared to the pure compound. Specifically, the simulated brain C_{max} increased from 37.40 µg/mL to 45.36 µg/mL, while the simulated AUC expanded from 31342.8 µg.min/mL to 35900 µg.min/mL after oral administration of 6 mg/kg in rats as shown in Fig. 5C. PBPK simulations suggest a potential increase in the expected brain exposure, likely due to improved solubility, sustained release, and better passing through the blood–brain barrier (BBB) [66].

Syringic acid is known for its neuroprotective, antioxidant, and anti-inflammatory effects, but its clinical utility is limited by diminished bioavailability and rapid systemic clearance [80]. The emulsome-based formulation may overcome these limitations by providing a lipidic nanocarrier system that could facilitate better BBB permeation and prolonged systemic circulation. Nanocarriers like emulsomes could enhance drug solubility and stability, protect the compound from enzymatic degradation, and promote enhanced permeability and retention effects in targeted organs such as the brain [81].

The increase in the simulated brain C_{max} and AUC values reflects improved pharmacokinetic profiles, which may allow for more effective therapeutic outcomes at lower or less frequent dosing. Such formulations are increasingly explored to treat neurodegenerative diseases and brain injuries, where effective drug delivery to the CNS is a considerable challenge.

It is worth noting that the plasma C_{max} for syringic acid increased from 154.98 ± 3.21 µg/mL to 278.73 ± 7.34 µg/mL, and the plasma AUC nearly doubled from 74412.2 ± 19.22 to 163174 ± 77.76 µg·min/mL after emulsomes formulation. The observed increase in plasma exposure suggests that emulsomes may improve the systemic bioavailability and circulation time of syringic acid. This enhanced profile could potentially facilitate more effective delivery to the brain; however, further studies are needed to confirm the extent of blood–brain barrier (BBB) penetration. Such improvements might ultimately support a more sustained therapeutic effect, potentially allowing for a reduction in dosage or frequency [82].

Conclusion

The present study describes the successful development and optimization of syringic acid–loaded emulsomes to address the limitations of poor aqueous solubility and low oral bioavailability of syringic acid. The optimized formulation exhibited high entrapment efficiency, nanoscale particle size, and adequate physicochemical stability, as reflected by its zeta potential. In addition, the formulation provided sustained drug release and significantly improved systemic relative bioavailability (~219%) compared with pure syringic acid, highlighting the potential of emulsomes as an efficient delivery platform.

Overall, these results strongly suggest that emulsomes is a promising strategy for supporting the potential of emulsomes as a delivery system for syringic acid, with predicted improvements in brain exposure that require further experimental validation, in the management of various

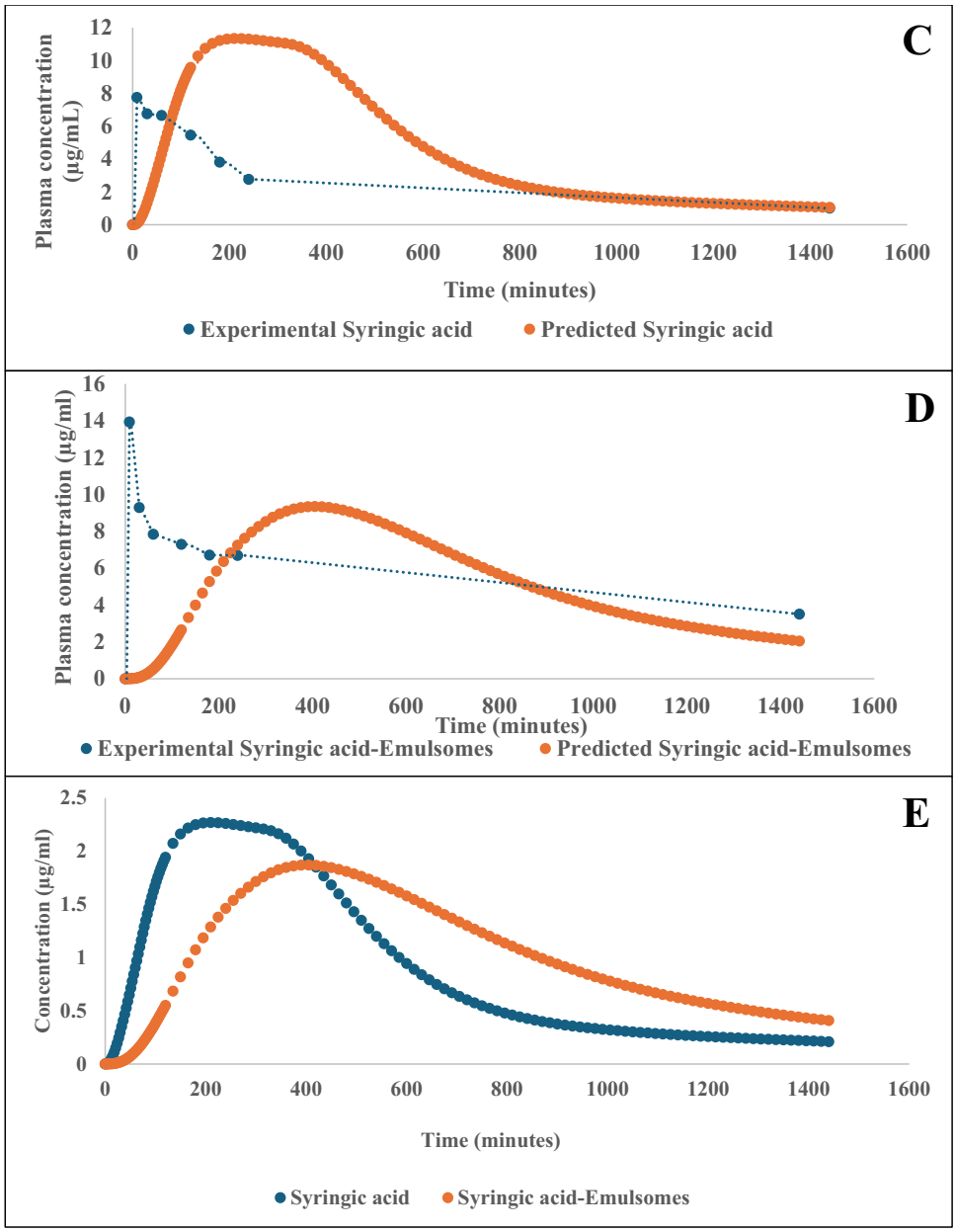

Fig. 5 Experimental versus observed plasma concentration–time profile of syringic acid following oral dose 6 mg/kg for **A**- unformulated syringic acid and **B**- syringic acid in emulsomes **C**-: Brain concentration–time profile of syringic acid

neurodegenerative diseases. While the PBPK simulations indicated an increased predicted brain exposure of syringic acid following emulsomal formulation, these findings remain model-based and do not constitute direct experimental confirmation of brain targeting. Future work will focus on conducting comprehensive *in-vivo* animal studies, which are currently ongoing, to further elucidate the biological performance of the developed system under physiological conditions. These studies aim to evaluate therapeutic efficacy and potential toxicity using appropriate animal models. In addition, future investigations will include quantitative residual solvent analysis, particularly for dichloromethane, using validated analytical techniques such as gas chromatography to ensure compliance with ICH guidelines for residual solvents and to further confirm the safety of the developed formulation. The outcomes of these studies are expected to provide essential insights into the safety, quality, and therapeutic potential of the formulation, thereby supporting its further optimization and advancing its translation toward clinical applications.

Supplementary Information The online version contains supplementary material available at https://doi.org/10.1208/s12249-026-03512-5.

Author Contributions All authors contributed to the study conceptualization and design. N.M. Sweed and M.H.S. Dawoud performed the *in-vitro* experiments and characterization, as well as data interpretation. M.H.

Elbishbishy conducted the extraction and isolation of gallic acid. Sara S. Saleh conducted the HPLC method development and validation. The original draft was written by N.M. Sweed and M.H.S. Dawoud, and all authors contributed to the critical revision and final approval of the manuscript.

Funding Open access funding provided by The Science, Technology & Innovation Funding Authority (STDF) in cooperation with The Egyptian Knowledge Bank (EKB).

Data Availability The corresponding author, Nabila M. Sweed, can provide the datasets created and/or analysed during the current work upon reasonable request.

Declarations

Ethics Approval The October University for Modern Sciences and Arts (MSA) faculty of Pharmacy's ethics committee authorized all techniques used in the performed animal experiments adhering to the ARRIVE criteria for laboratory animal usage (Approval number: PT83/REC83/2025PD).

Consent to Participate This study does not comprise any human subjects.

Consent for Publication This study does not comprise any human subjects.

Competing interests There are no pertinent financial or non-financial interests that the authors would want to declare.

References

1. Lee Y, Park K, Lee N, Paik H. Neuroprotective effects of Lactiplantibacillus plantarum and Pediococcus pentosaceus strains against oxidative stress via modulation of Nrf2-mediated antioxidation and anti-apoptosis. Brain Res [Internet]. 2025;1866(August):149925. Available from: https://doi.org/10.1016/j.brainres.2025.149925.
2. Niedzielska E, Smaga I, Gawlik M, Moniczewski A. Oxidative Stress in Neurodegenerative Diseases. Mol Neurobiol. 2016;54(6)(6):4094–125.
3. Zenin V, Ivanova J, Pugovkina N, Shatrova A, Aksenov N, Tyuryaeva I, et al. Redox Biology Resistance to H 2 O 2 -induced oxidative stress in human cells of different phenotypes. Redox Biol [Internet]. 2022;50:102245. Available from: https://doi.org/10.1016/j.redox.2022.102245.
4. Cao Y, Zhang L, Sun S, Yi Z, Jiang X, Jia D. Neuroprotective effects of syringic acid against OGD/R-induced injury in cultured hippocampal neuronal cells. Int J Mol Med. 2016;38(2):567–73.
5. Zhao Y, Dang M, Zhang W, Lei Y, Ramesh T, Priya Veeraraghavan V, et al. Neuroprotective effects of Syringic acid against aluminium chloride induced oxidative stress mediated neuroinflammation in rat model of Alzheimer's disease. J Funct Foods [Internet]. 2020;71(May):104009. Available from: https://doi.org/10.1016/j.jff.2020.104009.
6. Karamaæ M, Kosiñska A, Pegg RB. Comparison of radical-scavenging activities. Pol J Food Nutr Sci. 2005;14(2):165–9.
7. Rekha KR, Selvakumar GP, Sivakamasundari RI. Effects of syringic acid on chronic MPTP/probenecid induced motor dysfunction, dopaminergic markers expression and neuroinflammation in C57BL/6 mice. Biomed Aging Pathol [Internet]. 2014;4(2):95–104. Available from: https://doi.org/10.1016/j.biomag.2014.02.004.
8. Cao X, Zhou X, Wang Y, Gong T, Zhang ZR, Liu R, et al. Diblock- and triblock-copolymer based mixed micelles with high tumor penetration: In vitro and in vivo. J Mater Chem B. 2016;4(19):3216–24.
9. Srinivasulu C, Ramgopal M, Ramanjaneyulu G, Anuradha CM, Suresh KC. Syringic acid (SA) - A Review of Its Occurrence, Biosynthesis, Pharmacological and Industrial Importance. Biomed Pharmacother. 2018;108(August):547–57.
10. Liu Y, Sun C, Li W, Adu-frimpong M, Wang Q. Preparation and Characterization of Syringic Acid – Loaded TPGS Liposome with Enhanced Oral Bioavailability and In Vivo Antioxidant Efficiency. AAPS PharmSciTech. 2019;20(98):1–10.
11. Sun C, Li W, Ma P, Li Y, Zhu Y, Zhang H, et al. Development of TPGS/F127/F68 mixed polymeric micelles: Enhanced oral bioavailability and hepatoprotection of syringic acid against carbon tetrachloride-induced hepatotoxicity. Food Chem Toxicol [Internet]. 2020;137(October 2019):111126. Available from: https://doi.org/10.1016/j.fct.2020.111126.
12. Parmar A, Singh K, Bahadur A, Marangoni G, Bahadur P. Colloids and Surfaces B: Biointerfaces Interaction and solubilization of some phenolic antioxidants in Pluronic ® micelles. Colloids Surfaces B Biointerfaces [Internet]. 2011;86(2):319–26. Available from: https://doi.org/10.1016/j.colsurfb.2011.04.015.
13. Yusuf A, Almotairy ARZ, Henidi H, Alshehri OY, Aldughaim MS. Nanoparticles as Drug Delivery Systems: A Review of the Implication of Nanoparticles' Physicochemical Properties on Responses in Biological Systems. Polymers (Basel). 2023;15(7):449–507.
14. Dhiman N, Awasthi R, Sharma B, Kharkwal H. Lipid Nanoparticles as Carriers for Bioactive Delivery. Front Chem. 2021;9(April):1–19.
15. Annu, Sartaj A, Qamar Z, Md S, Alhakamy NA, Baboota S, et al. An Insight to Brain Targeting Utilizing Polymeric Nanoparticles: Effective Treatment Modalities for Neurological Disorders and Brain Tumor. Front Bioeng Biotechnol. 2022;10(February):1–18.
16. Li J, Cheng X, Chen Y, He W, Ni L, Xiong P, et al. Vitamin E TPGS modified liposomes enhance cellular uptake and targeted delivery of luteolin: An in vivo/in vitro evaluation. Int J Pharm. 2016;512(1):262–72.
17. Bhalekar M, Upadhaya P, Madgulkar A. Formulation and characterization of solid lipid nanoparticles for an anti-retroviral drug darunavir. Appl Nanosci. 2017;7(1):47–57.
18. Puri A, Loomis K, Smith B, Lee JH, Yavlovich A, Heldman E, et al. Lipid-based nanoparticles as pharmaceutical drug carriers: from concepts to clinic. Crit Rev Ther Drug Carrier Syst. 2009;26(6):523–80.
19. Salem LH, El-feky GS, Fahmy RH, El ON, Abdelbary A. Coated Lipidic Nanoparticles as a New Strategy for Enhancing Nose-to-Brain Delivery of a Hydrophilic Drug Molecule. J Pharm Sci [Internet]. 2020;1–15. Available from: https://doi.org/10.1016/j.xphs.2020.04.007.
20. Zhao Y, Cai C, Liu M, Zhao Y, Pei W, Chu X, et al. An organic solvent-free technology for the fabrication of albumin-based paclitaxel nanoparticles for effective cancer therapy. Colloids Surfaces B Biointerfaces [Internet]. 2019;183:110394. Available from: https://doi.org/10.1016/j.colsurfb.2019.110394.

21. Sun Y, Zhao Y, Teng S, Hao F, Zhang H, Meng F, et al. Folic acid receptor-targeted human serum albumin nanoparticle formulation of cabazitaxel for tumor therapy. Int J Nanomedicine. 2019;14:135–48.
22. Raza K, Katare OP, Setia A, Bhatia A, Singh B. Improved therapeutic performance of dithranol against psoriasis employing systematically optimized nanoemulsomes. J Microencapsul. 2013;30(3):225–36.
23. Elnady RE, Amin MM, Zakaria MY. A review on lipid - based nanocarriers mimicking chylomicron and their potential in drug delivery and targeting infectious and cancerous diseases. AAPS Open [Internet]. 2023;9(13):1–18. Available from: https://doi.org/10.1186/s41120-023-00080-x.
24. Sharma G, Thakur A, Singh J, Kaur G, Singh B, Raza K, et al. Investigating in-depth potential of lipid-engineered emulsomes of aceclofenac for the management of arthritis: A comprehensive preclinical study. Inorg Chem Commun [Internet]. 2025;172(113737):1–15. Available from: https://doi.org/10.1016/j.inoche.2024.113737.
25. Youssef YL, Megahed MA, El-Zaafarany GM, Osman R. Emulsomal nanovesicles: A platform for boosting the oral bioavailability and selective cytotoxicity of tamoxifen citrate towards breast cancer cells. J Drug Deliv Sci Technol [Internet]. 2025;108(March):106897. Available from: https://doi.org/10.1016/j.jddst.2025.106897.
26. Ucisik MH, Küpcü S, Schuster B, Sleytr UB. Characterization of CurcuEmulsomes : nanoformulation for enhanced solubility and delivery of curcumin. J Nanobiotechnology. 2013;11(37):1–13.
27. Correia AC, Monteiro AR, Silva R, Moreira JN, Lobo JMS, Silva AC. Lipid nanoparticles strategies to modify pharmacokinetics of central nervous system targeting drugs : Crossing or circumventing the blood – brain barrier (BBB) to manage neurological disorders. Adv Drug Deliv Rev [Internet]. 2022;189:114485. Available from: https://doi.org/10.1016/j.addr.2022.114485.
28. Gastaldi L, Battaglia L, Peira E, Chirio D, Muntoni E, Solazzi I, et al. Solid lipid nanoparticles as vehicles of drugs to the brain: Current state of the art. Eur J Pharm Biopharm. 2014;87(3):433–44.
29. Gupta J, Fatima MT, Islam Z, Khan RH, Uversky VN, Salahuddin P. Nanoparticle formulations in the diagnosis and therapy of Alzheimer's disease. Int J Biol Macromol [Internet]. 2019;130:515–26. Available from: https://doi.org/10.1016/j.ijbiomac.2019.02.156.
30. El-zaafarany GM, Soliman ME, Mansour S, Awad GAS. Identifying lipidic emulsomes for improved oxcarbazepine brain targeting : In vitro and rat in vivo studies. Int J Pharm [Internet]. 2016;503(1–2):127–40. Available from: https://doi.org/10.1016/j.ijpharm.2016.02.038.
31. Sawant D. Formulation and evaluation of sparfloxacin emulsomes-loaded thermosensitive in situ gel for ophthalmic delivery. J Sol-Gel Sci Technol. 2016;77(3):654–65.
32. Sweed NM, Elbishbishy MH, Yousry Y, Hisham H, Hany N, Mohamed A, et al. Journal of Drug Delivery Science and Technology Gallic acid-loaded chitosomes: A promising strategy to improve metabolic and endocrine function in PCOS. J Drug Deliv Sci Technol [Internet]. 2026;120(December 2025):108197. Available from: https://doi.org/10.1016/j.jddst.2026.108197.
33. Seju U, Kumar A, Sawant KK. Development and evaluation of olanzapine-loaded PLGA nanoparticles for nose-to-brain delivery: In vitro and in vivo studies. Acta Biomater. 2011;7(12):4169–76.
34. Radwan SAA, El-Maadawy WH, ElMeshad AN, Shoukri RA, Yousry C. Correction to: Impact of Reverse Micelle Loaded Lipid Nanocapsules on the Delivery of Gallic Acid into Activated Hepatic Stellate Cells: A Promising Therapeutic Approach for Hepatic Fibrosis (Pharm Res, https://doi.org/10.1007/s11095-020-02891). Pharm Res. 2020;37(11).
35. Vrignaud S, Anton N, Gayet P, Benoit JP, Saulnier P. Reverse micelle-loaded lipid nanocarriers: A novel drug delivery system for the sustained release of doxorubicin hydrochloride. Eur J Pharm Biopharm [Internet]. 2011;79(1):197–204. Available from: https://doi.org/10.1016/j.ejpb.2011.02.015.
36. Pavaloiu R, At FSHA, Hlevca C, At MSHA, Savoiu G, Osman S. Evaluation of drug release kinetics from polymeric nanoparticles loaded with poorly water-soluble APIs. Ovidius Univ Ann Chem. 2021;32(2):132–6.
37. Sweed NM, Elbalkiny HT, Magdy E, Ramadan M, Mahmoud S, Mohamed T, et al. Optimization of Linagliptin-loaded polymersomes via response surface methodology: A repurposed therapeutic strategy for hepatic encephalopathy prevention. J Drug Deliv Sci Technol [Internet]. 2025;108(January):106855. Available from: https://doi.org/10.1016/j.jddst.2025.106855.
38. Dawoud MHS, Zaafan MA, Saleh SS, Mannaa IM, Sweed NM. Response surface optimization of a cardioprotective compound through pharmacosomal drug delivery system: in vivo bioavailability and cardioprotective activity potential. Drug Deliv Transl Res [Internet]. 2023;13(9):2315–39. Available from: https://doi.org/10.1007/s13346-023-01315-w.
39. Farhan M, Rani P, Moledina F, George T, Tummala HP, Mallayasamy S. Application of Physiologically Based Pharmacokinetic Modeling of Lamotrigine Using PK-Sim in Predicting the Impact of Drug Interactions and Dosage Adjustment. J Pharmacol Pharmacother. 2022;13(2):160–6.
40. Gandevia L, Thotakura S, Mallayasamy S. Physiologically based pharmacokinetic model of valproic acid using PK-sim. Thai J Pharm Sci. 2023;47(2):1–8.
41. Alwaili MA, Eid TM, Abu-Almakarem AS, Alsirhani AM, Al-Sowayan NS, Aljarari RM, et al. Syringic Acid Alleviates Doxorubicin-Induced Hepatotoxicity Through PI3K/Akt-Mediated Nrf-2/HO-1 Signaling Pathways in Male Rats. Int J Mol Sci. 2025;26(16):1–22.
42. Ookawa Z, Higuchi Y, Fujita M, Sonoki T, Kamimura N, Masai E. Catabolic System of Syringic Acid, a Key Intermediate of Lignin-Derived Aromatic Compounds, via a Novel Linear Pathway in Pseudomonas sp. NGC7 . J Agric Food Chem. 2025;73(30):18899–913.
43. Peng J, Lu J, Shen Q, Zheng M, Luo X, Zhu W, et al. In silico site of metabolism prediction for human UGT-catalyzed reactions. Bioinformatics. 2014;30(3):398–405.
44. Gerhart JG, Watt KM, Edginton A, Wade KC, Salerno SN, Benjamin Jr DK, et al. Physiologically-based pharmacokinetic modeling of fluconazole using plasma and cerebrospinal fluid samples from preterm and term infants. CPT: Pharmacometrics & Systems Pharmacology. 2019;8(7):500–510.
45. Vyas SP, Subhedar R, Jain S. Development and characterization of emulsomes for sustained and targeted delivery of an antiviral agent to liver. J Pharm Pharmacol. 2010;58(3):321–6.
46. Elnady RE, Amin MM, Zakaria MY. Phytomedicinal flavonoid loaded phospholipid sheathed lipidic nano-carriers as a platform with boosted oral anti-mycobacterium activity. J Drug Deliv Sci Technol [Internet]. 2023;87(July):104775. Available from: https://doi.org/10.1016/j.jddst.2023.104775.
47. Khan N, Shah FA, Rana I, Ansari MM, Din F ud, Rizvi SZH, et al. Nanostructured lipid carriers-mediated brain delivery of carbamazepine for improved in vivo anticonvulsant and anxiolytic activity. Int J Pharm [Internet]. 2020;577(119033):1–10. Available from: https://doi.org/10.1016/j.ijpharm.2020.119033.
48. Bezerra MA, Santelli RE, Oliveira EP, Villar LS, Escaleira LA. Response surface methodology (RSM) as a tool for optimization in analytical chemistry. Talanta. 2008;76(5):965–77.

49. Chukwuka S, Chukwuneke JL, Chinwuko EC. Bio-lubricant production from Ozoro yellow oleander seeds and its industrial applications : Central composite design and python approach. Sci African [Internet]. 2025;29(May):e02827. Available from: https://doi.org/10.1016/j.sciaf.2025.e02827.
50. Mehnert W, Mäder K. Solid lipid nanoparticles: Production, characterization and applications. Adv Drug Deliv Rev [Internet]. 2012;64(SUPPL.):83–101. Available from: https://doi.org/10.1016/j.addr.2012.09.021.
51. Sila-On W, Vardhanabhuti N, Ongpipattanakul B, Kulvanich P. Influence of incorporation methods on partitioning behavior of lipophilic drugs into various phases of a parenteral lipid emulsion. AAPS PharmSciTech. 2008;9(2):684–92.
52. Malviya V. Preparation and evaluation of emulsomes as a drug delivery system for bifonazole. Indian J Pharm Educ Res. 2021;55(1):86–94.
53. Pulatsu E, De Nicola A, Pink D, Green NL, Adams C, Rousseau D, et al. Effect of alkyl chain length on the clustering of molten triacylglycerols. J Mol Liq [Internet]. 2025;423(December 2024):126993. Available from: https://doi.org/10.1016/j.molliq.2025.126993.
54. Bunjes H, Koch MHJ. Saturated phospholipids promote crystallization but slow down polymorphic transitions in triglyceride nanoparticles. J Control Release. 2005;107(2):229–43.
55. Nasr M, Mansour S, Mortada ND, El Shamy AA. Lipospheres as carriers for topical delivery of aceclofenac: preparation, characterization and in vivo evaluation. AAPS PharmSciTech. 2008;9(1):154–62.
56. Zhang B, Zhou X, Miao Y, Wang X, Yang Y, Zhang X, et al. Effect of phosphatidylcholine on the stability and lipolysis of nanoemulsion drug delivery systems. Int J Pharm [Internet]. 2020;583(April):119354. Available from: https://doi.org/10.1016/j.ijpharm.2020.119354.
57. Ishii F, Nii T. Lipid emulsions and lipid vesicles prepared from various phospholipids as drug carriers. In: Colloid and interface science in pharmaceutical research and development. Elsevier B.V.; 2014. p. 469–501. https://doi.org/10.1016/B978-0-444-62614-1.00007-7.
58. Kumarage T, Morris NB, Ashkar R. The effects of molecular and nanoscopic additives on phospholipid membranes. Front Phys. 2023;11(November):1–28.
59. Adrian Gołębiowski BB. Characterization of colloidal particles of a biological and metallic nature. Microchem J. 2023;191(108864):1–16.
60. Zhou X, Chen Z. Preparation and performance evaluation of emulsomes as a drug delivery system for silybin. Arch Pharm Res. 2015;38(12):2193–200.
61. Eita AS, Makky AMA, Anter A, Khalil IA. Atorvastatin-loaded emulsomes foam as a topical antifungal formulation. Int J Pharm X [Internet]. 2022;4:100140. Available from: https://doi.org/10.1016/j.ijpx.2022.100140.
62. Bunjes H, Unruh T. Characterization of lipid nanoparticles by differential scanning calorimetry, X-ray and neutron scattering ☆. Adv Drug Deliv Rev. 2007;59(6):379–402.
63. Müller RH, Radtke M, Wissing SAS. Solid lipid nanoparticles (SLN) and nanostructured lipid carriers (NLC) in cosmetic and dermatological preparations. Adv Drug Deliv Rev. 2002;54:S131-155.
64. Shalaby ES, Abdelhameed MF, El-Saied MA, Soliman HSM, Nagy AM, Elmotasem H. A triple strategy employing the revisited diosmin, nano emulsomes gel, and the topical route for psoriasis management in a UV-induced model. J Drug Deliv Sci Technol [Internet]. 2025;111(March):107194. Available from: https://doi.org/10.1016/j.jddst.2025.107194.
65. Zhou X, Chen Z. Preparation and performance evaluation of emulsomes as a drug delivery system for silybin. Arch Pharm Res. 2015;38(12):2193–2000.
66. Singh S, Khurana K, Chauhan SB, Singh I. Emulsomes: new lipidic carriers for drug delivery with special mention to brain drug transport. Futur J Pharm Sci [Internet]. 2023;9(1). Available from: https://doi.org/10.1186/s43094-023-00530-z.
67. Tiwari G, Tiwari R, Wal P, Wal A. Development and optimization of liposomes containing 5 fluorouracil and tretinoin for skin warts: 32 experimental design. Fabad J Pharm Sci. 2019;44(1):17–26.
68. Mohsen AM, AbouSamra MM, ElShebiney SA. Enhanced oral bioavailability and sustained delivery of glimepiride via niosomal encapsulation: in-vitro characterization and in-vivo evaluation. Drug Dev Ind Pharm [Internet]. 2017;43(8):1254–64. Available from: https://doi.org/10.1080/03639045.2017.1310224.
69. Hasan M, Elkhoury K, Kahn CJF, Arab-tehrany E, Linder M. Curcumin in Simulated Environments. Molecules. 2019;24:1–14.
70. Kamel R, AbouSamra MM, Afifi SM, Galal AF. Phyto-emulsomes as a novel nano-carrier for morine hydrate to combat leukemia: In vitro and pharmacokinetic study. J Drug Deliv Sci Technol [Internet]. 2022;75(April):103700. Available from: https://doi.org/10.1016/j.jddst.2022.103700.
71. Aldawsari HM, Badr-Eldin SM, Assiri NY, Alhakamy NA, Privitera A, Caraci F, et al. Surface-tailoring of emulsomes for boosting brain delivery of vinpocetine via intranasal route: in vitro optimization and in vivo pharmacokinetic assessment. Drug Deliv [Internet]. 2022;29(1):2671–84. Available from: https://doi.org/10.1080/10717544.2022.2110996.
72. Elsheikh MA, Rizk SA, Elnaggar YSR, Abdallah OY, Andrographolide AG. Nanoemulsomes for Enhanced Oral Bioavailability of the Anticancer Phytochemical Andrographolide : Characterization and Pharmacokinetics. AAPS PharmSciTech [Internet]. 2021;22(246):1–12. Available from: https://doi.org/10.1208/s12249-021-02112-9.
73. Du Y, Wang Z, Wang L, Gao M, Wang L, Gan C, et al. Simultaneous determination of seven phenolic acids in rat plasma using UHPLC-ESI-MS/MS after oral administration of echinacea purpurea extract. Molecules. 2017;22(9):1494.
74. Tao Y, Xu X, Yan J, Cai B. A sensitive UPLC–MS/MS method for simultaneous determination of polyphenols in rat plasma: Application to a pharmacokinetic study of dispensing granules and standard decoction of Cinnamomum cassia twigs. Biomed Chromatogr. 2019;33(7):1–8.
75. Kaur IP, Bhandari R, Bhandari S, Kakkar V. Potential of solid lipid nanoparticles in brain targeting. J Control Release. 2008;127(2):97–109.
76. Zakaria MY, Zaki I, Alhomrani M, Alamri AS, Abdulaziz O, Abourehab MAS. Boosting the anti MERS-CoV activity and oral bioavailability of resveratrol via PEG-stabilized emulsomal nanocarrier: Factorial design, in-vitro and in-vivo assessments. Drug Deliv [Internet]. 2022;29(1):3155–67. Available from: https://doi.org/10.1080/10717544.2022.2126028.
77. Sreeharsha N, Hiremath JG, Chilukuri S, Aitha RK, Al-Dhubiab BE, Venugopala KN, et al. An approach to enhance dissolution rate of tamoxifen citrate. Biomed Res Int. 2019;1:2161348.
78. Singh S, Khurana K, Chauhan SB, Singh I. Emulsomes: new lipidic carriers for drug delivery with special mention to brain drug transport. Futur J Pharm Sci [Internet]. 2023;9(1):78. Available from: https://doi.org/10.1186/s43094-023-00530-z.
79. Gill B, Singh J, Sharma V, Kumar SLH. Emulsomes: An emerging vesicular drug delivery system. Asian J Pharm. 2012;6(2):87–94.
80. Zhao Z, Yang Q, Sun Y, Ruan X. Unveiling the antioxidant and anti-inflammatory potential of syringic acid: mechanistic insights and pathway interactions. Front Pharmacol. 2025;16(July):1–22.

81. Abo El-Enin HA, Mostafa RE, Ahmed MF, Naguib IA, Abdelgawad MA, Ghoneim MM, et al. Assessment of Nasal-Brain-Targeting Efficiency of New Developed Mucoadhesive Emulsomes Encapsulating an Anti-Migraine Drug for Effective Treatment of One of the Major Psychiatric Disorders Symptoms. Pharmaceutics. 2022;14(2):1–18.

82. Stielow M, Witczyńska A, Kubryń N, Fijałkowski Ł, Nowaczyk J, Nowaczyk A. The bioavailability of drugs—the current state of knowledge. Molecules. 2023;28(24):8038.